Power Electronic Systems
Laboratory

IEEE Transactions on Power Electronics, Vol. 32, No. 4, pp. 3112-3127, April 2017

Analysis and Practical Relevance of CM/DM EMI Noise Separator Characteristics

F. Krismer,
S. Schroth,
H. Ertl,
K. Stoychev Kostov,
H. P. Nee,
J. W. Kolar

Eidgenössische Technische Hochschule Zürich
Swiss Federal Institute of Technology Zurich

Analysis and Practical Relevance of CM/DM EMI Noise Separator Characteristics

Florian Krismer, *Member, IEEE*, Sebastian Schroth, Hans Ertl, *Member, IEEE*, Konstantin Stoychev Kostov, *Senior Member, IEEE*, Hans-Peter Nee, *Senior Member, IEEE*, and Johann Walter Kolar, *Fellow, IEEE*

***Abstract*—This work investigates sources of measurement errors that result for common mode/differential mode (CM/DM) separators in a practical measurement environment, with a particular focus on the recently presented input impedance criterion for CM/DM separators, derives the respective analytical expressions, and employs a detailed analytical model to verify the obtained findings. Furthermore, a method is derived, which determines the worst-case measurement error by reason of cross coupling for given measured DM and CM output voltage components. Based on an example, this work illustrates how the obtained expressions can be advantageously used in a computer program to automatically decide whether a particular spectral measurement component represents a useful measurement result or if it is strongly affected by cross coupling (CM to DM and DM to CM). Finally, the paper presents the realization and accompanying experimental results of an active CM/DM separator, which allows for low realization effort and features competitive separation capabilities ($DMTR/CMRR > 50$ dB and $CMTR/DMRR > 42$ dB for frequencies up to 10 MHz).**

***Index Terms*—Analog processing circuits, electromagnetic compatibility, electromagnetic interference (EMI), frequency domain analysis, measurement errors, power electronics, voltage measurement.**

Nomenclature

V	Rms value of a considered voltage.
$\underline{V} = V\mathrm{e}^{\mathrm{j}\varphi}$	Phasor corresponding to a sinusoidal voltage, $v(t) = \sqrt{2}\,V\cos(\omega t + \varphi)$, at given angular frequency, ω (alternative time-domain signals are considered by means of Fourier analysis).
$\underline{Z} = R + \mathrm{j}X$	Complex impedance.
$\underline{V}_{\mathrm{sep,l}}$, $\underline{V}_{\mathrm{sep,n}}$	Phasors of the input voltages of the CM/DM separator.
$\underline{V}_{\mathrm{sep,DM}}$, $\underline{V}_{\mathrm{sep,CM}}$	Phasors of the DM and CM components corresponding to the separator's input voltages.
$\underline{V}_{\mathrm{out,DM}}$, $\underline{V}_{\mathrm{out,CM}}$	Phasors of the output voltages of the separator.
$DMTR = \lvert\frac{\underline{V}_{\mathrm{out,DM}}}{\underline{V}_{\mathrm{sep,DM}}}\rvert$	Differential mode transmission ratio.
$CMTR = \lvert\frac{\underline{V}_{\mathrm{out,CM}}}{\underline{V}_{\mathrm{sep,CM}}}\rvert$	Common mode transmission ratio.
$CMRR = \lvert\frac{\underline{V}_{\mathrm{out,DM}}}{\underline{V}_{\mathrm{sep,CM}}}\rvert$	Common mode rejection ratio.
$DMRR = \lvert\frac{\underline{V}_{\mathrm{out,CM}}}{\underline{V}_{\mathrm{sep,DM}}}\rvert$	Differential mode rejection ratio.
e_{DM}, e_{CM}	DM and CM gain errors due to CM/DM separator's input impedances.
f_{DM}, f_{CM}	Indicators assessing measurement errors due to cross coupling (DM and CM).

(N.B.: This list summarizes only the most important symbols; DMTR, CMTR, CMRR, and DMRR are defined according to [2].)

Manuscript received February 2, 2016; revised April 15, 2016; accepted May 27, 2016. Date of publication June 9, 2016; date of current version January 20, 2017. This paper is a revised and extended version of an initial conference contribution [1]. Recommended for publication by Associate Editor Dr. R. Redl.

F. Krismer and J. W. Kolar are with the Power Electronic Systems Laboratory, Swiss Federal Institute of Technology, Zurich 8092, Switzerland (e-mail: krismer@lem.ee.ethz.ch; kolar@lem.ee.ethz.ch).

S. Schroth is with the ebm-papst Mulfingen GmbH & Co. KG, Mulfingen 74673, Germany (e-mail: Sebastian.Schroth@de.ebmpapst.com).

H. Ertl is with the Vienna University of Technology, Wien 1040, Austria (e-mail: johann.ertl@tuwien.ac.at).

K. S. Kostov is with the Acreo Swedish ICT AB, Kista 164 40, Sweden (e-mail: konstantin.kostov@acreo.se).

H.-P. Nee is with the KTH Royal Institute of Technology, Stockholm 114 28, Sweden (e-mail: hansi@kth.se).

Color versions of one or more of the figures in this paper are available online at http://ieeexplore.ieee.org.

Digital Object Identifier 10.1109/TPEL.2016.2579267

I. Introduction

The practical applicability of different common mode/differential mode (CM/DM) separators, used to determine CM and DM components of the conducted electromagnetic interference (EMI) noise generated by a switched mode power supply, is investigated. In this context, the single-phase power factor correction (PFC) rectifier of the variable speed drive system depicted in Fig. 1(a), which is designed for 230 V/50 Hz mains and features a maximum output power of 500 W, serves as a suitable platform for experimental verification. In order to limit the maximum allowable levels of conducted EMI noise in each mains phase according to IEC 61000-6-3 [3], an EMI filter, e.g., designed according to [4], is inserted between the mains connection and the power converter as shown in Fig. 1(a). The effectiveness of the EMI filter is verified with the measurement setup depicted in Fig. 1(b) [5], which employs line impedance stabilization networks (LISNs), depicted in Fig. 1(c), in each phase in order to achieve reproducible measurements, i.e., independent of the mains impedance. The device under test (DUT) in Fig. 1(b) is modeled according to [6].

Initial measurements of conducted EMI noise often reveal insufficient filter attenuation, in particular at high frequencies above 1 MHz. In this context, the question arises how actual deficiencies of the EMI filter can be resolved in a systematic way. Since the EMI filter employs essentially different filter components to suppress DM and CM EMI noise, a common approach for a diagnostic inspection is to separate the conducted EMI

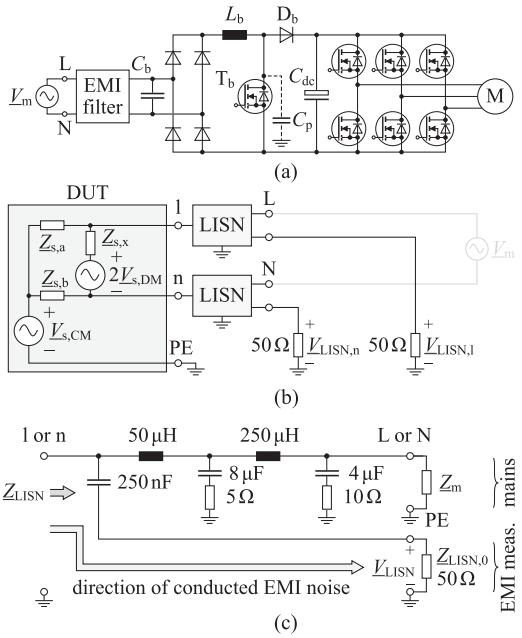

Fig. 1. (a) Considered single-phase PFC rectifier; the depicted inverter powers an electric machine. (b) Setup used to measure conducted electromagnetic interference (EMI) noise levels. (c) Schematic drawing of a commonly used LISN.

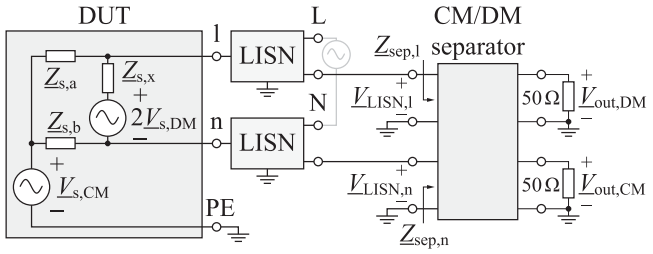

Fig. 2. Setup used to measure DM and CM components of the conducted EMI noise. The CM/DM separator is directly connected to the outputs of the LISNs.

noise into DM and CM noise. Direct measurement of DM and CM EMI noise is feasible with the measurement setup depicted in Fig. 2, which employs a CM/DM separator and facilitates the measurements of the conducted DM and CM EMI noise without and with EMI filter. With the results obtained from these measurements it is possible to trace reasons for insufficient filter attenuations, cf. [7], inspect the effectiveness of a novel filter topology [8] or design strategy [9] by means of experiments, or specifically verify analytical methods related to investigations of conducted EMI noise, e.g., [10] for a boost-type PFC rectifier.

A literature review reveals numerous different realizations of single-phase CM/DM separators, which can be categorized according to the list below.

1) *Passive separators* suppress either DM or CM component and preserve the remaining CM or DM component, respectively. Examples are CM/DM separators realized with resistor networks [11], broadband transformers [2], [12]–[14], or power combiners [15].
2) *Active separators* employ operational amplifiers to determine DM and CM components (realized in [16]; circuits of active CM/DM separators are shown in [17]–[19]).
3) *Digital or software solutions* [17], [20], [21], e.g., with the use of digital oscilloscopes.
4) *Direct measurement* of CM and DM components with current probes [22].

CM/DM separators are subject to limited CM and DM separation capabilities. In this context, the CM and DM transmission and rejection ratios (CMTR, DMTR, CMRR, and DMRR, cf. Section II) are criteria used for evaluating CM/DM separators [2].[1] In addition to limited separation capabilities of the separators themselves, however, also interactions at the interfaces between the LISNs' output ports and the separator's input ports in Fig. 2 may deteriorate the accuracy of the measured output voltages [6].

The first part of the presented work investigates the implications of characteristic properties of CM/DM separators, i.e., input-side impedance characteristics and CMTR, DMTR, CMRR, and DMRR values, on the measurement results in a well-defined practical measurement environment. In this context, the contribution of an initial conference contribution [1] of this paper is the derivation of the expected measurement error due to the eventually present impedance mismatch at the separator's input side. The present paper now extends [1] by a novel method for calculating two indicators, f_{DM} and f_{CM}, which assess how strong the DM to CM and CM to DM cross couplings affect the measured DM and CM spectral components. Based on examples, it is shown how the derived indicators can be used to automatically separate meaningful spectral measurement components from components that are subject to severe measurement errors. Compared to [1], the measurements of conducted EMI have been repeated with an improved EMI filter in order to mitigate a resonance of the CM filter at 13 MHz.

The second part of this work focuses on an improved active CM/DM separator circuit, which is an extended version of the circuits realized in [16] and shown in [17] and has first been demonstrated in [1]. This paper, in addition, details the mode of operation and the realization specifics of the implemented separator. The considered circuit can be easily reproduced (without need for tuning), features competitive noise separation capabilities with $DMTR/CMRR > 50$ dB and $CMTR/DMRR > 42$ dB for frequencies up to 10 MHz, and may, depending on particular needs, represent an attractive alternative to conventional passive CM/DM separators. The measurement of the frequency responses of CMTR, DMTR, CMRR, and DMRR has been conducted with power splitters instead of the S-parameter method used in [1], which is justified in the Appendix.

The paper begins with a summary on the common properties of CM/DM separators in Section II. This facilitates the derivation of expressions for the errors expected in a practical measurement environment in Section III, i.e., the errors due to

[1]Cross coupling is also expected for the direct measurement method with current probes, because the measurement result obtained with a current probe slightly depends on the position of the conductor, due to parasitic couplings. Since the positions of both conductors are not identical, also the direct measurement with current probes is prone to cross coupling. The corresponding frequency responses of CMTR, DMTR, CMRR, and DMRR can be determined according to Appendix B.

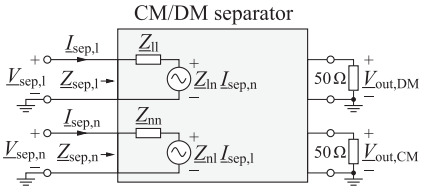

Fig. 3. Characterization of the input ports of a CM/DM separator based on impedance matrix coefficients [6].

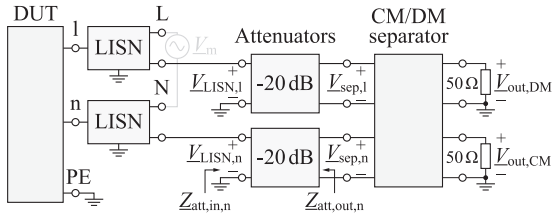

Fig. 4. EMI measurement setup including precision attenuators, here with an attenuation of 20 dB, between the LISNs and the CM/DM separator.

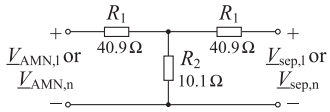

Fig. 5. Resistances of a 50 Ω T-type attenuator network with 20 dB attenuation.

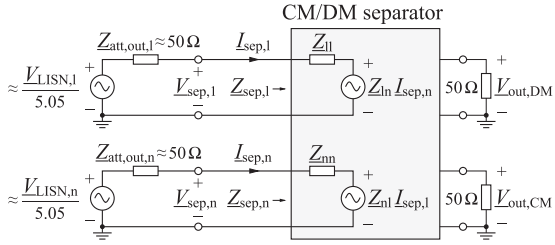

Fig. 6. Simplified model used to estimate the DM and CM components' measurement errors in the setup of Fig. 4 by reason of $\underline{\mathbf{Z}}_{\mathrm{sep}} \neq \mathbf{Z}_{\mathrm{sep,ideal}}$.

impedance mismatch in Section III-A, the implications of tolerances on measurement errors in Section III-B, the derivation of f_{DM} and f_{CM} in Section III-C, and the evaluation with experimental data in Section III-D. Section IV details the active noise separator and Section V summarizes the findings of this work.

II. Properties of Single-Phase CM/DM Separators

Any single-phase CM/DM separator senses two input voltages at its input ports, e.g., $\underline{V}_{\mathrm{sep,l}}$ and $\underline{V}_{\mathrm{sep,n}}$ in Fig. 3, and processes the measured voltages in order to determine DM and CM components, which, in case of ideal separation, directly provides the values of the input-side DM and CM components

$$\begin{aligned}\underline{V}_{\mathrm{sep,DM}} &= \frac{\underline{V}_{\mathrm{sep,l}} - \underline{V}_{\mathrm{sep,n}}}{2}\\ \underline{V}_{\mathrm{sep,CM}} &= \frac{\underline{V}_{\mathrm{sep,l}} + \underline{V}_{\mathrm{sep,n}}}{2}\end{aligned} \tag{1}$$

at its output ports, i.e., $\underline{V}_{\mathrm{out,DM}} = \underline{V}_{\mathrm{sep,DM}}$ and $\underline{V}_{\mathrm{out,CM}} = \underline{V}_{\mathrm{sep,CM}}$.

In a practical realization, the accuracy achievable for $\underline{V}_{\mathrm{out,DM}}$ and $\underline{V}_{\mathrm{out,CM}}$ is limited. This is partly due to an unsuitable input impedance matrix of the CM/DM separator

$$\underline{\mathbf{Z}}_{\mathrm{sep}} = \begin{pmatrix} \underline{Z}_{\mathrm{ll}} & \underline{Z}_{\mathrm{ln}} \\ \underline{Z}_{\mathrm{nl}} & \underline{Z}_{\mathrm{nn}} \end{pmatrix} \neq \underline{\mathbf{Z}}_{\mathrm{sep,ideal}} = \begin{pmatrix} 50\,\Omega & 0 \\ 0 & 50\,\Omega \end{pmatrix} \tag{2}$$

cf. Fig. 3, which introduces errors to $\underline{V}_{\mathrm{sep,l}}$ and $\underline{V}_{\mathrm{sep,n}}$ [6]. Further measurement errors arise from inaccurate processing of the measured voltages, commonly accounted for with gain errors (DMTR and/or CMTR different to 0 dB) and cross coupling (CMRR and/or DMRR greater than zero, i.e., greater than $-\infty$ dB). DMTR, CMTR, CMRR, and DMRR allow for the estimation of the maximum output voltages including gain errors and cross coupling, which is detailed in Section III-B2.

III. Measurement Errors in a Practical Setup

A. Impact of $\underline{\mathbf{Z}}_{\mathrm{sep}}$ on the Measurement Result

Fig. 2 depicts the basic measurement setup used to determine DM and CM EMI noise. A more practical setup, however, employs precision attenuators between the LISNs and the noise separator, according to Fig. 4, to terminate the LISNs with almost constant load impedances, $\underline{Z}_{\mathrm{att,in,l}}$ and $\underline{Z}_{\mathrm{att,in,n}}$, close to 50 Ω. The T-type attenuator network depicted in Fig. 5, for example, features an attenuation of 20 dB and provides an input impedance between 49 Ω and 51 Ω, depending on whether the attenuator's output is terminated with a short-circuit or an open-circuit, respectively.[2] The shown 20 dB-attenuator, in addition, provides a well-defined voltage source at its output side, e.g., the attenuator connected to the l-phase provides an open-circuit voltage of $\underline{V}_{\mathrm{LISN,l}}/5.05$ with an inner impedance of $\underline{Z}_{\mathrm{att,out,l}} \approx 50\,\Omega$. Thus, with the separator model depicted in Fig. 3, the circuit diagram of Fig. 6 can be established. In the first step, the circuit of Fig. 6 facilitates the calculation of the separator's input voltages, $\underline{V}_{\mathrm{sep,l}}$ and $\underline{V}_{\mathrm{sep,n}}$. This, in the second step, enables the calculation of the DM and CM voltages, $\underline{V}_{\mathrm{out,DM}}$ and $\underline{V}_{\mathrm{out,CM}}$, that are applied to the test receiver, which, in the third step, allows for the calculation of the implications of $\underline{\mathbf{Z}}_{\mathrm{sep}} \neq \underline{\mathbf{Z}}_{\mathrm{sep,ideal}}$, cf. (2), on the measurement result.

The separator's input voltages can be calculated by solving the corresponding equation system

$$\begin{aligned}\frac{\underline{V}_{\mathrm{wLISN,l}}}{5.05} &= (\underline{Z}_{\mathrm{att,out,l}} + \underline{Z}_{\mathrm{ll}})\underline{I}_{\mathrm{sep,l}} + \underline{Z}_{\mathrm{ln}}\underline{I}_{\mathrm{sep,n}}\\ \frac{\underline{V}_{\mathrm{LISN,n}}}{5.05} &= (\underline{Z}_{\mathrm{att,out,n}} + \underline{Z}_{\mathrm{nn}})\underline{I}_{\mathrm{sep,n}} + \underline{Z}_{\mathrm{nl}}\underline{I}_{\mathrm{sep,l}}.\end{aligned} \tag{3}$$

with respect to $\underline{I}_{\mathrm{sep,l}}$ and $\underline{I}_{\mathrm{sep,n}}$ and inserting the solutions to

$$\begin{aligned}\underline{V}_{\mathrm{sep,l}} &= \underline{Z}_{\mathrm{ll}}\underline{I}_{\mathrm{sep,l}} + \underline{Z}_{\mathrm{ln}}\underline{I}_{\mathrm{sep,n}}\\ \underline{V}_{\mathrm{sep,n}} &= \underline{Z}_{\mathrm{nn}}\underline{I}_{\mathrm{sep,n}} + \underline{Z}_{\mathrm{nl}}\underline{I}_{\mathrm{sep,l}}\end{aligned} \tag{4}$$

[2]Still, sufficient voltage level is available at the input of the test receiver, since modern test receivers feature useful operation for input voltages as low as ≈ 15 dBμV, which is considerably less than the allowable limits of conducted EMI noise defined in [3] minus 20 dB.

which gives

$$\underline{V}_{\mathrm{sep,l}} = \frac{\underline{V}_{\mathrm{LISN,n}}\underline{Z}_{\mathrm{ln}}\underline{Z}_{\mathrm{att,out,l}}+\underline{V}_{\mathrm{LISN,l}}\left[\underline{Z}_{\mathrm{ll}}\left(\underline{Z}_{\mathrm{nn}}+\underline{Z}_{\mathrm{att,out,l}}\right)-\underline{Z}_{\mathrm{ln}}\underline{Z}_{\mathrm{nl}}\right]}{5.05\left[\left(\underline{Z}_{\mathrm{ll}}+\underline{Z}_{\mathrm{att,out,l}}\right)\left(\underline{Z}_{\mathrm{nn}}+\underline{Z}_{\mathrm{att,out,n}}\right)-\underline{Z}_{\mathrm{ln}}\underline{Z}_{\mathrm{nl}}\right]} \tag{5}$$

$$\underline{V}_{\mathrm{sep,n}} = \frac{\underline{V}_{\mathrm{LISN,l}}\underline{Z}_{\mathrm{nl}}\underline{Z}_{\mathrm{att,out,n}}+\underline{V}_{\mathrm{LISN,n}}\left[\underline{Z}_{\mathrm{nn}}\left(\underline{Z}_{\mathrm{ll}}+\underline{Z}_{\mathrm{att,out,n}}\right)-\underline{Z}_{\mathrm{ln}}\underline{Z}_{\mathrm{nl}}\right]}{5.05\left[\left(\underline{Z}_{\mathrm{ll}}+\underline{Z}_{\mathrm{att,out,l}}\right)\left(\underline{Z}_{\mathrm{nn}}+\underline{Z}_{\mathrm{att,out,n}}\right)-\underline{Z}_{\mathrm{ln}}\underline{Z}_{\mathrm{nl}}\right]}. \tag{6}$$

In these two equations, the LISN output voltages $\underline{V}_{\mathrm{LISN,n}}$ and $\underline{V}_{\mathrm{LISN,l}}$ are advantageously replaced by the corresponding CM and DM components

$$\begin{aligned}\underline{V}_{\mathrm{LISN,l}} &= \underline{V}_{\mathrm{LISN,CM}} + \underline{V}_{\mathrm{LISN,DM}}\\ \underline{V}_{\mathrm{LISN,n}} &= \underline{V}_{\mathrm{LISN,CM}} - \underline{V}_{\mathrm{LISN,DM}}.\end{aligned} \tag{7}$$

The expressions resulting for $\underline{V}_{\mathrm{sep,l}}$ and $\underline{V}_{\mathrm{sep,n}}$ are processed according to (1) in order to determine the CM and DM components of the separator's input voltages, $\underline{V}_{\mathrm{sep,DM}}$ and $\underline{V}_{\mathrm{sep,CM}}$. Finally, the expressions obtained for $\underline{V}_{\mathrm{sep,DM}}$ and $\underline{V}_{\mathrm{sep,CM}}$ are processed using the definitions for DMTR, CMTR, CMRR, and DMRR, given in the Nomenclature at the beginning of this work, in order to calculate the maximum values expected at the separator's output ports, $\max\left(V_{\mathrm{out,DM}}\right)$ and $\max\left(V_{\mathrm{out,CM}}\right)$, cf. (14). Even though this calculation is straightforward, large expressions result for $\max\left(V_{\mathrm{out,DM}}\right)$ and $\max\left(V_{\mathrm{out,CM}}\right)$. In a first approach, the assumptions listed below are made to allow for a simplified calculation of the measurement error expected for $\underline{\mathbf{Z}}_{\mathrm{sep}} \neq \underline{\mathbf{Z}}_{\mathrm{sep,ideal}}$. At the end of this section, the obtained result is verified in the course of a more in-depth investigation:

1) ideal transfer ratios: $DMTR = CMTR = 0$ dB;
2) no cross couplings: $DMRR \to -\infty$ dB and $CMRR \to -\infty$ dB;
3) setup is ideally symmetric: $\underline{Z}_{\mathrm{att,out,l}} = \underline{Z}_{\mathrm{att,out,n}}$, $\underline{Z}_{\mathrm{ll}} = \underline{Z}_{\mathrm{nn}}$, and $\underline{Z}_{\mathrm{ln}} = \underline{Z}_{\mathrm{nl}}$.

With these assumptions $\underline{V}_{\mathrm{out,DM}}$ and $\underline{V}_{\mathrm{out,CM}}$ can be calculated

$$\begin{aligned}\underline{V}_{\mathrm{out,DM}} &= \frac{\underline{V}_{\mathrm{LISN,DM}}}{5.05}\,\frac{\underline{Z}_{\mathrm{ll}}-\underline{Z}_{\mathrm{ln}}}{\underline{Z}_{\mathrm{att,out,l}}+\underline{Z}_{\mathrm{ll}}-\underline{Z}_{\mathrm{ln}}}\\ \underline{V}_{\mathrm{out,CM}} &= \frac{\underline{V}_{\mathrm{LISN,CM}}}{5.05}\,\frac{\underline{Z}_{\mathrm{ll}}+\underline{Z}_{\mathrm{ln}}}{\underline{Z}_{\mathrm{att,out,l}}+\underline{Z}_{\mathrm{ll}}+\underline{Z}_{\mathrm{ln}}}.\end{aligned} \tag{8}$$

It is important to note that the CM and DM components are decoupled in (8) (and, thus, in the setup depicted in Fig. 4), i.e., $V_{\mathrm{out,DM}}$ does not depend on $V_{\mathrm{LISN,CM}}$ and $V_{\mathrm{out,CM}}$ does not depend on $V_{\mathrm{LISN,DM}}$. Therefore, only complex DM and CM gain errors (magnitude and phase shift)

$$\begin{aligned}\underline{e}_{\mathrm{DM}} &= \frac{\underline{V}_{\mathrm{out,DM}}\big|_{\underline{\mathbf{Z}}_{\mathrm{sep}}\neq\underline{\mathbf{Z}}_{\mathrm{sep,ideal}}}}{\underline{V}_{\mathrm{out,DM}}\big|_{\underline{\mathbf{Z}}_{\mathrm{sep}}=\underline{\mathbf{Z}}_{\mathrm{sep,ideal}}}},\\ \underline{e}_{\mathrm{CM}} &= \frac{\underline{V}_{\mathrm{out,CM}}\big|_{\underline{\mathbf{Z}}_{\mathrm{sep}}\neq\underline{\mathbf{Z}}_{\mathrm{sep,ideal}}}}{\underline{V}_{\mathrm{out,CM}}\big|_{\underline{\mathbf{Z}}_{\mathrm{sep}}=\underline{\mathbf{Z}}_{\mathrm{sep,ideal}}}}\end{aligned} \tag{9}$$

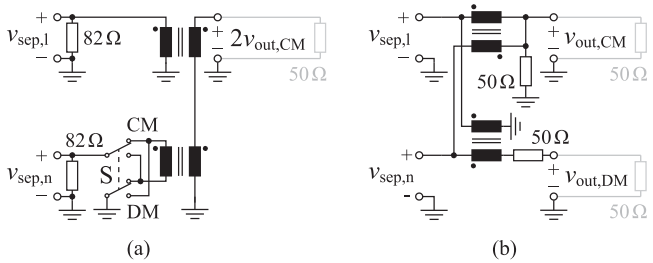

Fig. 7. (a) Passive separator proposed in [12], which violates the input impedance criterion (2). (b) The passive separator proposed in [2] fulfills (2) [6].

are to be expected for a separator with a nonideal input impedance matrix if the measurement setup shown in Fig. 4 is employed and if the above listed assumptions are met. With (8) the absolute values of the DM and CM errors are:[3]

$$\begin{aligned}e_{\mathrm{DM}} &= \left|\frac{\underline{Z}_{\mathrm{ll}}-\underline{Z}_{\mathrm{ln}}}{\underline{Z}_{\mathrm{att,out,l}}+\underline{Z}_{\mathrm{ll}}-\underline{Z}_{\mathrm{ln}}}\,\frac{50\,\Omega+\underline{Z}_{\mathrm{att,out,l}}}{50\,\Omega}\right|\\ e_{\mathrm{CM}} &= \left|\frac{\underline{Z}_{\mathrm{ll}}+\underline{Z}_{\mathrm{ln}}}{\underline{Z}_{\mathrm{att,out,l}}+\underline{Z}_{\mathrm{ll}}+\underline{Z}_{\mathrm{ln}}}\,\frac{50\,\Omega+\underline{Z}_{\mathrm{att,out,l}}}{50\,\Omega}\right|.\end{aligned} \tag{10}$$

A prominent CM/DM separator which does not fulfill the input impedance criterion defined with (2) is the CM/DM separator proposed by Paul and Hardin in [12], depicted in Fig. 7(a). The input impedance matrix of this separator is as follows:

$$\underline{\mathbf{Z}}_{\mathrm{sep,Paul}} = \begin{pmatrix} 50.6\,\Omega & \pm 31.4\,\Omega \\ \pm 31.4\,\Omega & 50.6\,\Omega \end{pmatrix}. \tag{11}$$

The $\pm$-sign denotes whether the circuit separates DM or CM, i.e., the sign is positive for DM separation and negative for CM separation. In combination with (10), same error factors result for DM and CM separation, $e_{\mathrm{DM}} = e_{\mathrm{CM}} = 0.555$, which corresponds to a gain error of -5.1 dB compared to a DM/CM separator that facilitates an ideal input impedance matrix, e.g., the separator presented by Wang *et al.* in [2] and depicted in Fig. 7(b).

According to the result (10) derived above, any symmetric input matrix impedance of a CM/DM separator is expected to not cause CM/DM cross coupling if the measurement setup is completely symmetric, too. A real measurement setup, however, may not be fully symmetric. Still, the resulting measurement error can be calculated for a more realistic measurement environment, too, using the more complete model depicted in Fig. 8. This includes the EMI noise source model presented in Fig. 9(a) in [6],[4] the CM/DM separator model of Fig. 3, and LISN and attenuator networks (N.B.: the cascade matrices model LISNs,

[3]Since, IEC 61000-6-3 [3] only specifies limits for the amplitudes of conducted EMI, the phase shifts introduced by nonideal input impedance matrixes, $\arg(\underline{e}_{\mathrm{DM}})$ and $\arg(\underline{e}_{\mathrm{DM}})$, are not considered in this work. N.B.: The peak values of conducted EMI are expected to be independent of phase shift errors during processing, since same peak values result when the phasors of all spectral components in the measured 9 kHz frequency band of the EMI test receiver are in phase [23]. Considerations of the implications of phase shifts on the results obtained with quasi-peak and average detectors are, however, out of the scope of this work.

[4]The DM current source with inner impedance has been replaced by a DM voltage source with inner impedance.

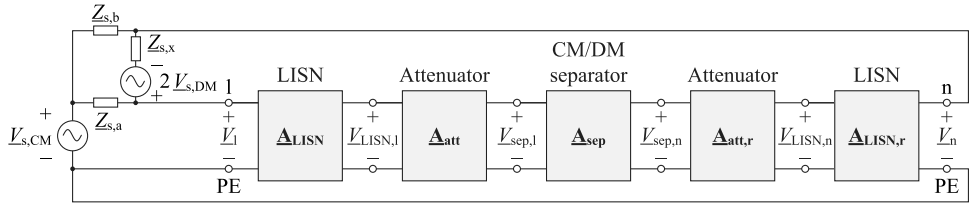

Fig. 8. Detailed model used to verify e_{DM} and e_{CM} obtained for the simplified model, cf. (10).

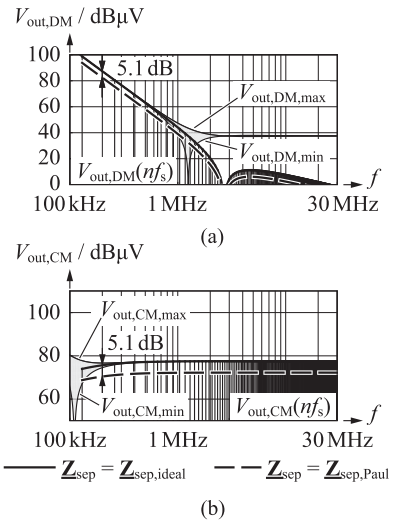

Fig. 9. (a) DM and (b) CM components calculated for the network of Fig. 8 and for two different CM/DM separators, i.e., a separator with $\underline{\mathbf{Z}}_{\mathrm{sep}} = \underline{\mathbf{Z}}_{\mathrm{sep,ideal}}$ (solid curves) and the separator of [12] with $\underline{\mathbf{Z}}_{\mathrm{sep,Paul}} \neq \underline{\mathbf{Z}}_{\mathrm{sep,ideal}}$ (dashed curves). The depicted shaded areas denote measurement uncertainties determined for $DMRR = -30$ dB, $CMRR = -40$ dB, and $DMTR = CMTR = 0$ dB, cf. Section III-B2.

TABLE I
DESIGN PARAMETERS, OPERATING CONDITIONS, AND COMPONENT VALUES OF THE INVESTIGATED PFC RECTIFIER (WITHOUT EMI FILTER)

Designator	*Value*	*Description*
V_{m}	230 V	Mains voltage
V_{dc}	430 V	Dc link voltage
P_{dc}	500 W	Output power (resistive load)
f_s	130 kHz	Switching frequency
T_b	IDH08S60C	SiC power diode (CREE)
D_b	SPW35N60C3	CoolMOS power MOSFET (Infineon)
L_b	465 μH	Inductance of the boost converter (Kaschke, custom made, ferrite core)
C_b	470 nF	Input capacitance of the boost converter
C_{p}	15 pF	Parasitic capacitance between earth and the drain of the MOSFET

attenuators, and CM/DM separator; $\underline{\mathbf{A}}_{\mathrm{att,r}}$ and $\underline{\mathbf{A}}_{\mathrm{LISN,r}}$ denote the reverse of $\underline{\mathbf{A}}_{\mathrm{att}}$ and $\underline{\mathbf{A}}_{\mathrm{LISN}}$, respectively).

In the course of a modeled example, the PFC rectifier circuit of Fig. 1(a), specified in Table I, and without EMI filter (in order to investigate the performance of CM/DM separators in case of an asymmetric DUT, i.e., for $\underline{Z}_{\mathrm{s,a}}$ being considerably different to $\underline{Z}_{\mathrm{s,b}}$ in Fig. 8) serves as a basis for configuring the EMI noise

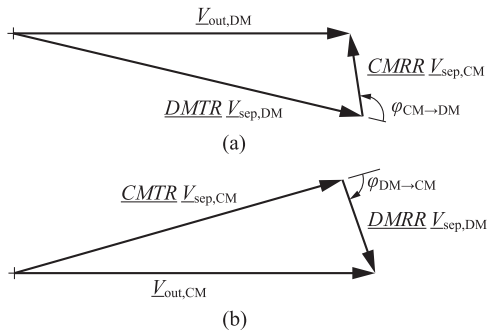

Fig. 10. Phasors of the separator's output voltages for given phasors of DM and CM input voltage components and cross coupling: (a) DM, (b) CM.

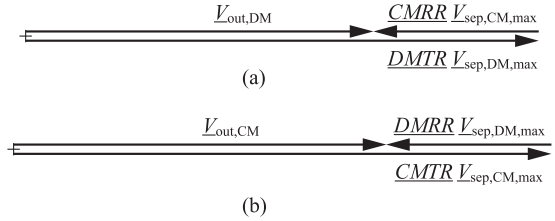

Fig. 11. Phasor diagrams illustrating how the maximum DM and CM voltage components at the separator's input ports are reconstructed for known output voltages: (a) DM, (b) CM.

source (from [6], [7])

$$\begin{aligned}
\underline{V}_{\mathrm{s}}(nf_s) &= \frac{1}{n}\sqrt{\frac{4}{\pi}V_{\mathrm{m,pk}}V_0 - V_{\mathrm{m,pk}}^2} \quad \forall\, n \in \mathbb{N} \\
\underline{V}_{\mathrm{s,DM}}(nf_s) &= \frac{\underline{V}_{\mathrm{s}}(nf_s)}{2} \cdot \frac{1}{1-(2\pi nf_s)^2 L_b C_b} \\
\underline{V}_{\mathrm{s,CM}} &= \underline{V}_{\mathrm{s}}\, \mathrm{e}^{\mathrm{j}\pi} \\
\underline{Z}_{\mathrm{s,x}}(nf_s) &= \frac{\mathrm{j}2\pi nf_s L_b}{1-(2\pi nf_s)^2 L_b C_b} \\
\underline{Z}_{\mathrm{s,a}}(nf_s) &\to \infty \\
\underline{Z}_{\mathrm{s,b}}(nf_s) &= \frac{1}{2\pi nf_s C_{\mathrm{p}}}.
\end{aligned} \tag{12}$$

In (12) the noise source is modeled according to [7], which is based on the EMI noise source model proposed and investigated in [24]. For the derivations of the expressions for $\underline{V}_{\mathrm{s,DM}}$, $\underline{V}_{\mathrm{s,CM}}$, $\underline{Z}_{\mathrm{s,a}}$, $\underline{Z}_{\mathrm{s,b}}$, and $\underline{Z}_{\mathrm{s,x}}$, ideal diodes and MOSFET, infinite dc-link capacitance, and operation in the positive mains half-period are assumed.

Fig. 9(a) and (b) depicts the RMS values of the DM and CM output voltages calculated for this PFC rectifier, using

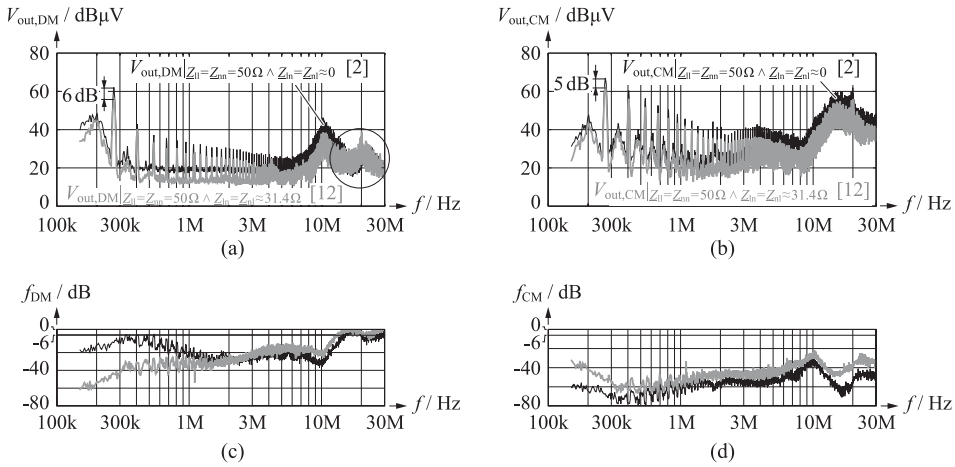

Fig. 12. (a) DM and (b) CM components measured according to Fig. 4, with the separators of [2] ($\underline{\mathbf{Z}}_{\mathrm{sep,Wang}} = \underline{\mathbf{Z}}_{\mathrm{sep,ideal}}$) and [12] ($\underline{\mathbf{Z}}_{\mathrm{sep,Paul}} \neq \underline{\mathbf{Z}}_{\mathrm{sep,ideal}}$; a gain of 6 dB, inherent to the separator of [12], cf. Fig. 7(a), has been removed by means of initial calibration). In order to allow for a comparison with known limits of conducted EMI, 20 dB have been added to the actual measurement result. (c) and (d) Values of f_{DM} and f_{CM}, cf. (33) and (34), indicating how much cross coupling influences the DM and CM measurement results, respectively, cf. Section III-C, (36), and (37).

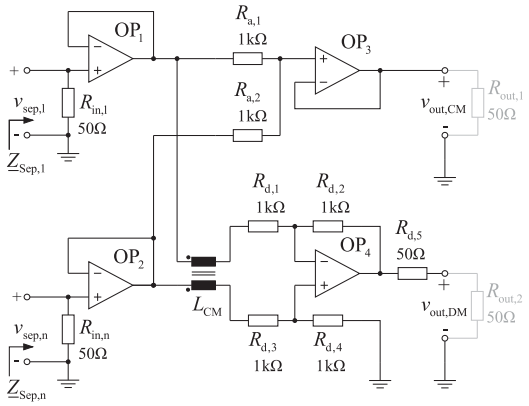

Fig. 13. Schematic drawing of the presented active CM/DM separator.

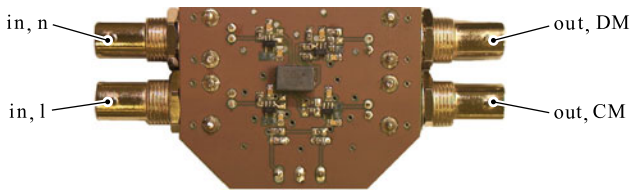

Fig. 14. Picture of the active CM/DM separator revealing the low complexity of this circuit. A 9 V-battery powers the separator.

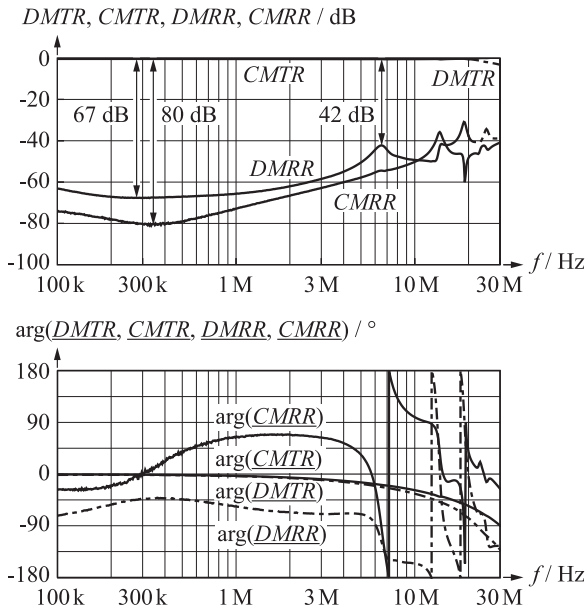

Fig. 15. Amplitude and phase responses of DMTR, CMTR, DMRR, and CMRR of the considered active CM/DM separator depicted in Fig. 13 (separator only), measured with power splitters, cf. Appendix B. This separator features $DMTR/CMRR > 50$ dB and $CMTR/DMRR > 42$ dB for frequencies up to 10 MHz.

the network of Fig. 8 with 20 dB precision attenuators and CM/DM separators with different input impedance matrices. The respective calculation has been parameterized according to Table I and (12), considers a PFC rectifier without EMI filter to include the implications of asymmetric EMI noise source impedances on the calculated DM and CM components, and assumes ideal boost inductance and input capacitance in order to emphasize on the measurement error that results for a nonideal input impedance matrix of the CM/DM separator. EMI filter and parasitic effects, including nonideal frequency responses of L_b and C_b, are considered in the measurement results presented in Section III-D and Fig. 12.

The calculated results are in good agreement with (10): The separators with $\underline{\mathbf{Z}}_{\mathrm{sep}} = \underline{\mathbf{Z}}_{\mathrm{sep,ideal}}$ (solid curves) and $\underline{\mathbf{Z}}_{\mathrm{sep}} = \underline{\mathbf{Z}}_{\mathrm{sep,Paul}}$ (dashed curves) return the same CM and DM components except for a gain error of -5.1 dB introduced by the circuit of [12].

B. Implications of Limited Accuracies on Measurement Errors

The results presented in the previous Section III-A consider LISNs and precision attenuators with ideal component values and CM/DM separators featuring ideal separation, i.e., $DMTR = CMTR = 0$ dB, $DMRR \to -\infty$ dB, and $CMRR \to -\infty$ dB. Precision attenuators, realized with

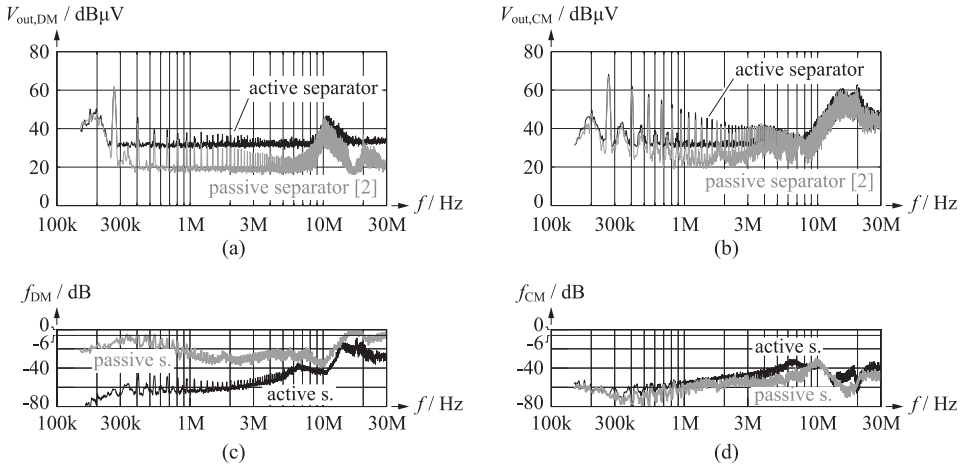

Fig. 16. (a) and (b) Comparison of the DM and CM components measured according to Fig. 4, with the active CM/DM separator (gray curve) and the passive CM/DM separators of [2] (black curve). 20 dB have been added to the measurement result to allow for comparison with known EMI limits. (c) and (d) Values of f_{DM} and f_{CM} corresponding to the measurement results depicted in (a) and (b).

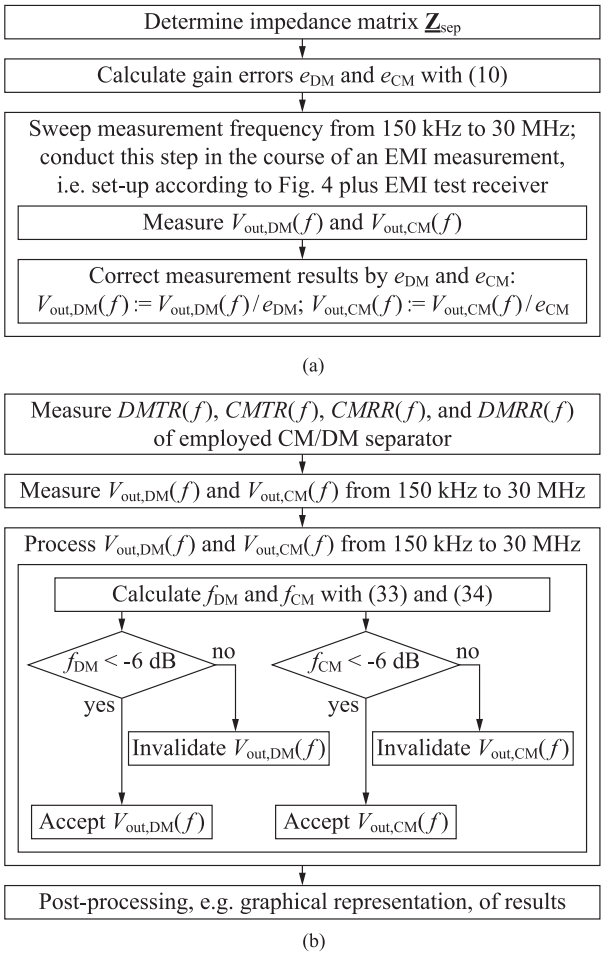

Fig. 17. Flow charts summarizing possible uses of the expressions elaborated in this work: (a) calculation and application of the gain errors e_{DM} and e_{CM}, (b) assessment of measured CM and DM components by means of f_{DM} and f_{CM}.

low-tolerance components, are readily available. Commercially available realizations of LISNs, however, may be subject to fairly high-input impedance tolerances [5]. The maximum mea-

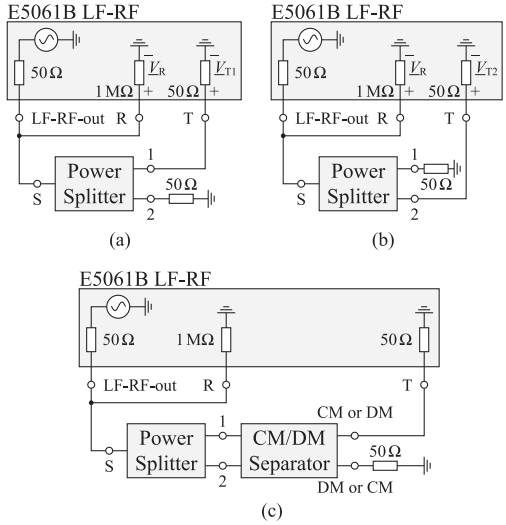

Fig. 18. (a) and (b) Setup used to determine the output characteristics of the power splitters, $\underline{\mathrm{G}}_{\mathrm{CM}}$ and $\underline{\mathrm{G}}_{\mathrm{DM}}$, with (38): (a) measurement of output signal at port 1, (b) output signal at port 2. (c) Setup used to measure DMTR, CMTR, CMRR, and DMRR of the CM/DM separators according to [30] with the network analyzer E5061B with option LF-RF [31].

surement errors expected for standard LISN realizations are detailed in Section III-B1. The measurement errors introduced by reason of limited CMRR- and DMRR-values of CM/DM separators are investigated in Section III-B2.

1) Tolerances Specified for the LISN: According to [5], the allowable tolerances of magnitude and phase shift of the LISN's input impedance, $\underline{Z}_{\mathrm{LISN}}$, are $\pm 20\%$ and $\pm 11.5°$, respectively. Thus, if only a DM or a CM component is applied to the inputs of the two LISNs, both, CM and DM, components result at the LISNs' outputs. A simplified calculation of the attenuation of the corresponding cross coupling reveals

$$Att_{\mathrm{LISN,CM}\leftrightarrow\mathrm{DM}} = \frac{\underline{\mathrm{Z}}_{\mathrm{LISN,0,l}} + \underline{\mathrm{Z}}_{\mathrm{LISN,0,n}}}{\underline{\mathrm{Z}}_{\mathrm{LISN,0,l}} - \underline{\mathrm{Z}}_{\mathrm{LISN,0,n}}} \tag{13}$$

which, by reason of the high-tolerance values, gives an unacceptably low value of the minimum cross-coupling attenuation of

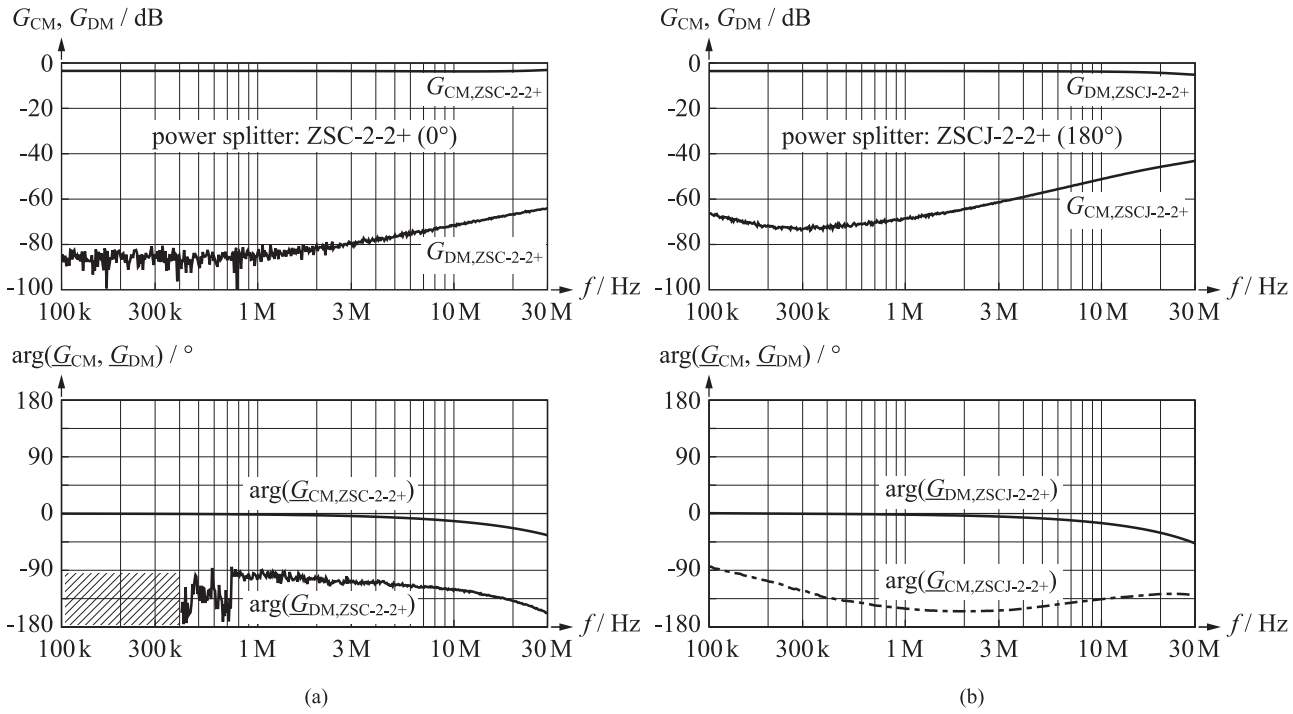

Fig. 19. Transfer functions of the power splitters: (a) ZSC-2-2+ (0°) and (b) ZSCJ-2-2+ (180°), both manufactured by mini circuits.

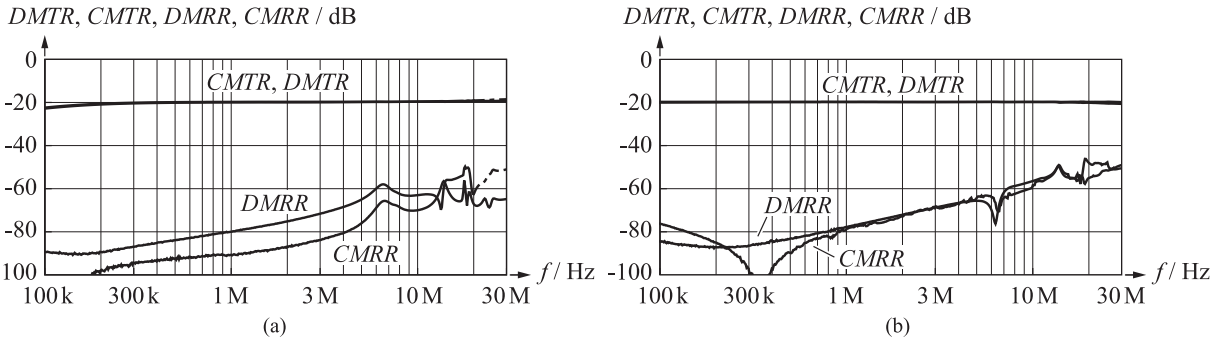

Fig. 20. DMTR, CMTR, CMRR, and DMRR of the series connection of LISNs, 20 dB attenuators, and active separator: (a) measurement with power splitters, (b) measurement with S-parameters.

11 dB.[5] For this reason, two identical LISN networks need to be employed, which may either be achieved with the realization of two identical LISN networks using high-precision components [1] or by verifying the suitability of available LISN networks by means of measurements. This work pursues the second approach, using two commercial LISNs of same type (ENV216 manufactured by Rohde&Schwarz). The measurement results depicted in Figs. 20 and 22 in Appendix B and obtained for the series connection of LISNs, attenuators, and separator according to Fig. 4, confirm the practicability of this approach.

2) CM/DM Separators with Limited Values of CMRR and DMRR: Limited values of DMTR, CMTR, CMRR, and DMRR lead to an uncertainty of the measured DM and CM output voltages. Based on the corresponding definitions given in the Nomenclature it is straightforward to derive the respective limits

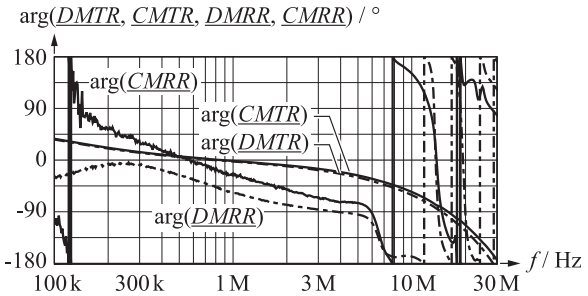

Fig. 21. Phase responses of DMTR, CMTR, CMRR, and DMRR (series connection of LISNs, 20 dB attenuators, and active separator; measured with power splitters).

[5] In the considered frequency range, 150 kHz $\leq f \leq$ 30 MHz, the above given tolerances are considered to approximately apply to the termination resistance connected to the measurement port of the LISN, $\underline{Z}_{\mathrm{LISN},0}$, since the LISN effectively redirects high-frequency currents to the measurement port, cf. Fig. 1(c).

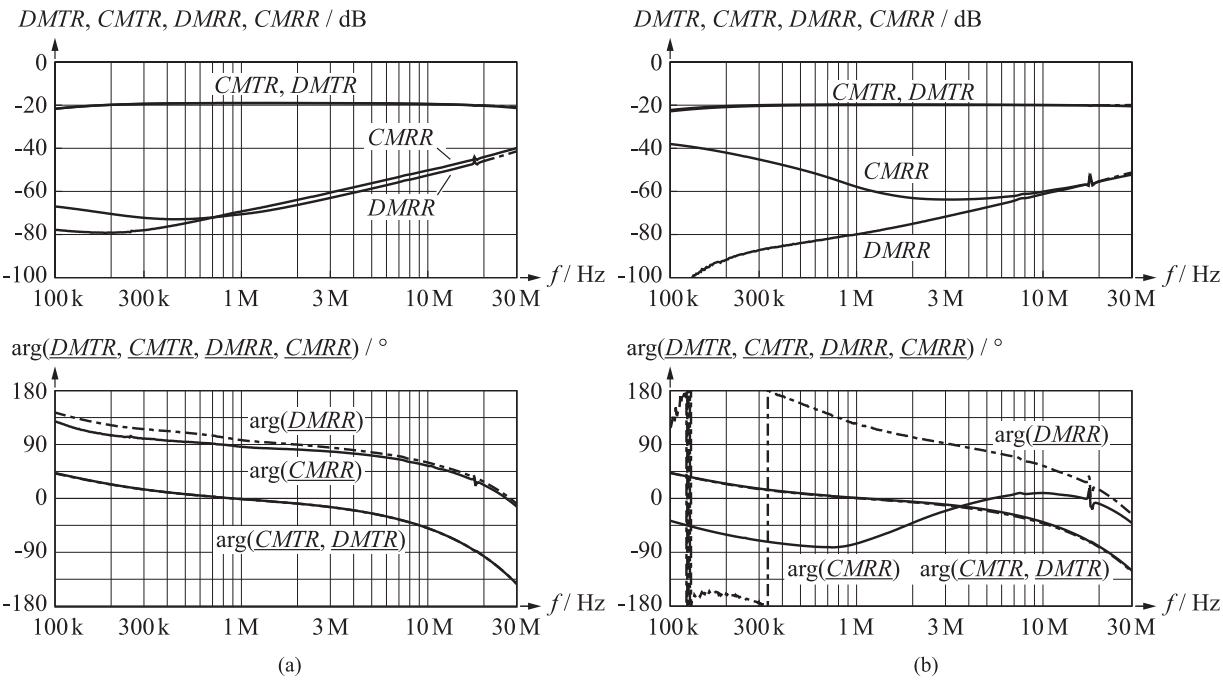

Fig. 22. Amplitude and phase responses of DMTR, CMTR, CMRR, and DMRR of the series connection of LISNs, 20 dB attenuators, and passive separators: (a) passive separator presented in [12]; (b) passive separator of [2].

for $V_{\mathrm{out,DM}}$ and $V_{\mathrm{out,CM}}$

$$V_{\mathrm{out,DM,min}} \leq V_{\mathrm{out,DM}} \leq V_{\mathrm{out,DM,max}}$$
$$V_{\mathrm{out,CM,min}} \leq V_{\mathrm{out,CM}} \leq V_{\mathrm{out,CM,max}}. \quad (14)$$

The results for $V_{\mathrm{out,DM,min}}$ and $V_{\mathrm{out,DM,max}}$, for example, are:

$$V_{\mathrm{out,DM,min}} = |DMTR\, V_{\mathrm{sep,DM}} - CMRR\, V_{\mathrm{sep,CM}}|$$
$$V_{\mathrm{out,DM,max}} = DMTR\, V_{\mathrm{sep,DM}} + CMRR\, V_{\mathrm{sep,CM}}. \quad (15)$$

The shaded areas depicted in Fig. 9, plotted for $DMRR = -30$ dB, $CMRR = -40$ dB, and $DMTR = CMTR = 0$ dB, denote points where the inequalities (14) hold true. In this figure, the value of $V_{\mathrm{out,DM}}$ becomes increasingly inaccurate for increasing frequencies and $f > 1$ MHz, due to $V_{\mathrm{sep,DM}}(f) < V_{\mathrm{sep,CM}}(f) CMRR/DMTR$, cf. (15) [$V_{\mathrm{sep,DM}}(f) = V_{\mathrm{out,DM}}(f)$ and $V_{\mathrm{sep,CM}}(f) = V_{\mathrm{out,CM}}(f)$ would apply for an ideal separator]. Similarly, $V_{\mathrm{out,CM}}$ becomes increasingly inaccurate for decreasing frequencies and $f < 200$ kHz, due to $V_{\mathrm{sep,CM}}(f) < V_{\mathrm{sep,DM}}(f) DMRR/CMTR$.

C. Implications of Cross Couplings on the Measurement Results

Equations (14) and (15) are restricted to the calculation of the ranges of the separator's CM and DM output voltages for known magnitudes of the input voltage components $V_{\mathrm{sep,DM}}$ and $V_{\mathrm{sep,CM}}$. In a practical setup, however, the actually present CM and DM voltages at the input of the separator are unknown and sought for. This section presents how the maximum magnitudes of the input voltage components $V_{\mathrm{sep,DM}}$ and $V_{\mathrm{sep,CM}}$ can be estimated for measured *output* voltage magnitudes $V_{\mathrm{out,DM}}$ and $V_{\mathrm{out,CM}}$.

According to the phasor diagrams depicted in Fig. 10, the output voltages are, at a given frequency, composed of the weighted CM and DM input voltage components:

$$\underline{V}_{\mathrm{out,DM}} = \underline{DMTR}\, \underline{V}_{\mathrm{sep,DM}} + \underline{CMRR}\, \underline{V}_{\mathrm{sep,CM}} \quad (16)$$
$$\underline{V}_{\mathrm{out,CM}} = \underline{CMTR}\, \underline{V}_{\mathrm{sep,CM}} + \underline{DMRR}\, \underline{V}_{\mathrm{sep,DM}}. \quad (17)$$

The EMI test receiver, however, only provides the magnitudes $V_{\mathrm{out,DM}}$ and $V_{\mathrm{out,CM}}$. The respective phasings are unknown, which makes it impossible to determine the phase shifts $\varphi_{\mathrm{CM}\to\mathrm{DM}}$ and $\varphi_{\mathrm{DM}\to\mathrm{CM}}$ shown in Fig. 10. Subsequently, $V_{\mathrm{sep,DM}}$ and $V_{\mathrm{sep,CM}}$ cannot be obtained from the equation system given with (16) and (17). Still, with the considerations presented in the following, it is possible to estimate the maximum values of $V_{\mathrm{sep,DM}}$ and $V_{\mathrm{sep,CM}}$.

According to the phasor diagram depicted in Fig. 11(a) the maximum value of $V_{\mathrm{sep,DM}}$ (denoted $V_{\mathrm{sep,DM,max}}$) is present if the phase shift between the phasors $\underline{DMTR}\ \underline{V}_{\mathrm{sep,DM}}$ and $\underline{CMRR}\ \underline{V}_{\mathrm{sep,CM}}$ is 180° and if the maximum CM voltage is assumed to be present at the input of the separator, i.e., $|\underline{DMTR}\ \underline{V}_{\mathrm{sep,DM,max}}| = |\underline{V}_{\mathrm{out,DM}}| + |\underline{CMRR}\ \underline{V}_{\mathrm{sep,CM,max}}|$ applies. The same applies to $V_{\mathrm{sep,CM,max}}$, cf. Fig. 11(b). With the assumed phase relations in these worst case scenarios, the further analysis can be confined to the magnitudes of voltages and transmission and rejection ratios. Due to $V_{\mathrm{out,DM}} > 0$ and $V_{\mathrm{out,CM}} > 0$, four different cases can be distinguished regarding the estimation of $\underline{V}_{\mathrm{sep,DM,max}}$ and $\underline{V}_{\mathrm{sep,CM,max}}$, depending on whether the evaluation of $DMTR\ V_{\mathrm{sep,DM,max}} - CMRR\ V_{\mathrm{sep,CM,max}}$ and $CMTR\, V_{\mathrm{sep,CM,max}} - DMRR\, V_{\mathrm{sep,DM,max}}$ returns positive or negative results. An investigation of all four cases reveals that, for a useful CM/DM separator with $DMTR > CMRR$ and

$CMTR > DMRR$, the maximum input values $V_{\mathrm{sep,DM,max}}$ and $V_{\mathrm{sep,CM,max}}$ are obtained for the case depicted in Fig. 11. This assumes that the condition

$$DMTR\,V_{\mathrm{sep,DM,max}} > CMRR\,V_{\mathrm{sep,CM,max}} \wedge CMTR\,V_{\mathrm{sep,CM,max}} > DMRR\,V_{\mathrm{sep,DM,max}} \quad (18)$$

holds true, which is verified below with (23)–(25).

With (18) and Fig. 11 the relations between the separator's maximum input voltages and its output voltages become

$$V_{\mathrm{out,DM}} = DMTR\,V_{\mathrm{sep,DM,max}} - CMRR\,V_{\mathrm{sep,CM,max}} \quad (19)$$

$$V_{\mathrm{out,CM}} = CMTR\,V_{\mathrm{sep,CM,max}} - DMRR\,V_{\mathrm{sep,DM,max}}. \quad (20)$$

Solving this equation system with respect to $V_{\mathrm{sep,DM,max}}$ and $V_{\mathrm{sep,CM,max}}$ gives

$$V_{\mathrm{sep,DM,max}} = \frac{CMTR\,V_{\mathrm{out,DM}} + CMRR\,V_{\mathrm{out,CM}}}{DMTR\,CMTR - DMRR\,CMRR} \approx \frac{V_{\mathrm{out,DM}}}{DMTR} + \frac{V_{\mathrm{out,CM}}\,CMRR}{DMTR\,CMTR} \quad (21)$$

$$V_{\mathrm{sep,CM,max}} = \frac{DMTR\,V_{\mathrm{out,CM}} + DMRR\,V_{\mathrm{out,DM}}}{DMTR\,CMTR - DMRR\,CMRR} \approx \frac{V_{\mathrm{out,CM}}}{CMTR} + \frac{V_{\mathrm{out,DM}}\,DMRR}{DMTR\,CMTR} \quad (22)$$

(the approximated results for $V_{\mathrm{sep,DM,max}}$ and $V_{\mathrm{sep,CM,max}}$ assume $DMTR\,CMTR \gg DMRR\,CMRR$).

The above result can now be used to check whether the condition (18) is fulfilled. For this, the exact solutions of (21) and (22) are inserted to (18), which, with

$$DMTR\,V_{\mathrm{sep,DM,max}} = \frac{DMTR\,CMTR\,V_{\mathrm{out,DM}} + DMTR\,CMRR\,V_{\mathrm{out,CM}}}{DMTR\,CMTR - DMRR\,CMRR} \quad (23)$$

$$CMRR\,V_{\mathrm{sep,CM,max}} = \frac{DMTR\,CMRR\,V_{\mathrm{out,CM}} + DMRR\,CMRR\,V_{\mathrm{out,DM}}}{DMTR\,CMTR - DMRR\,CMRR} \quad (24)$$

(and similar expressions for $CMTR\ V_{\mathrm{sep,CM,max}}$ and $DMRR\,V_{\mathrm{sep,DM,max}}$) give

$$V_{\mathrm{out,DM}} > 0 \ \wedge\ V_{\mathrm{out,CM}} > 0 \quad (25)$$

i.e., (18) holds true for meaningful, positive, magnitudes of the separator's output voltages.

With (21) and (22) it is possible to derive a criterion, which enables the evaluation of the implications of cross couplings on the measured CM and DM components, i.e., if $V_{\mathrm{sep,CM}}$ strongly affects $V_{\mathrm{out,DM}}$ and if $V_{\mathrm{sep,DM}}$ strongly affects $V_{\mathrm{out,CM}}$. For this derivation the following two extreme conditions, where only CM or DM components are present at the separator's input, are considered first:

Case I: $V_{\mathrm{sep,DM}} = 0$ und $V_{\mathrm{sep,CM}} > 0$;

Case II: $V_{\mathrm{sep,DM}} > 0$ und $V_{\mathrm{sep,CM}} = 0$.

Based on (19) and (20), simple expressions for $V_{\mathrm{out,DM}}$ and $V_{\mathrm{out,CM}}$ result for case I

$$V_{\mathrm{out,DM}} = CMRR\,V_{\mathrm{sep,CM}} \quad (26)$$

$$V_{\mathrm{out,CM}} = CMTR\,V_{\mathrm{sep,CM}}. \quad (27)$$

With the approximations given in (21) and (22) for $DMTR\,CMTR \gg DMRR\,CMRR$, the results for $V_{\mathrm{sep,DM,max}}$ and $V_{\mathrm{sep,CM,max}}$ corresponding to case I are obtained with (21), (22), and (27)

$$V_{\mathrm{sep,DM,max,I}} \approx V_{\mathrm{sep,CM}}\frac{CMRR}{DMTR} + V_{\mathrm{sep,CM}}\frac{CMRR}{DMTR} = 2V_{\mathrm{sep,CM}}\frac{CMRR}{DMTR} = \frac{2V_{\mathrm{out,CM}}\,CMRR}{DMTR\,CMTR} \quad (28)$$

$$V_{\mathrm{sep,CM,max,I}} \approx V_{\mathrm{sep,CM}} + V_{\mathrm{sep,CM}}\frac{DMRR\,CMRR}{DMTR\,CMTR} \approx V_{\mathrm{sep,CM}} = \frac{V_{\mathrm{out,CM}}}{CMTR}. \quad (29)$$

Thus, for case I, the CM component at the output of the separator represents a useful reconstruction of the input side CM component, cf. (29), however, the output side DM component is subject to cross coupling. The estimated input side DM component

$$V_{\mathrm{sep,DM,max,I}} \approx (V_{\mathrm{sep,CM}} + V_{\mathrm{sep,CM}})\frac{CMRR}{DMTR} = \underbrace{V_{\mathrm{sep,CM}}\frac{CMRR}{DMTR}}_{\text{due to cross coupling}} + \underbrace{V_{\mathrm{out,\,CM}}\frac{CMRR}{DMTR\,CMTR}}_{\text{due to reconstruction with (21)}} \neq 0 \quad (30)$$

reflects this situation: the first summand in (30) stems from the actual cross coupling, the second summand from the reconstruction based on (21) and the result is different to the originally considered input side DM voltage of $V_{\mathrm{sep,DM}} = 0$. Similar findings results for case II

$$V_{\mathrm{sep,DM,max,II}} \approx V_{\mathrm{sep,DM}} + V_{\mathrm{sep,DM}}\frac{DMRR\,CMRR}{DMTR\,CMTR} \approx V_{\mathrm{sep,DM}} = \frac{V_{\mathrm{out,DM}}}{DMTR} \quad (31)$$

$$V_{\mathrm{sep,CM,max,II}} \approx V_{\mathrm{sep,DM}}\frac{DMRR}{CMTR} + V_{\mathrm{sep,DM}}\frac{DMRR}{CMTR} = 2V_{\mathrm{sep,DM}}\frac{DMRR}{CMTR} = \frac{2V_{\mathrm{out,\,DM}}\,DMRR}{DMTR\,CMTR}. \quad (32)$$

Based on these considerations a possible criterion for evaluating how strong the actually present (but unknown) CM and DM voltage components at the separator's input ports, $V_{\mathrm{sep,CM}}$ and $V_{\mathrm{sep,DM}}$, affect the reconstructed input voltage components, $V_{\mathrm{sep,DM,max}}$ und $V_{\mathrm{sep,CM,max}}$, can be defined. For this, each worst case reconstructed input voltage component, resulting in case of pure cross coupling, is related to the corresponding completely reconstructed input voltage component, i.e., the results (28) and (32) are divided by the results (21) and (22), respectively

$$f_{\mathrm{DM}} = \frac{V_{\mathrm{sep,DM,max,I}}}{V_{\mathrm{sep,DM,max}}} = \frac{2V_{\mathrm{out,CM}}\,\frac{CMRR}{CMTR}}{V_{\mathrm{out,DM}} + V_{\mathrm{out,CM}}\,\frac{CMRR}{CMTR}} \quad (33)$$

$$f_{\mathrm{CM}} = \frac{V_{\mathrm{sep,CM,max,II}}}{V_{\mathrm{sep,CM,max}}} = \frac{2V_{\mathrm{out,DM}}\,\frac{DMRR}{DMTR}}{V_{\mathrm{out,CM}} + V_{\mathrm{out,DM}}\,\frac{DMRR}{DMTR}}. \quad (34)$$

N.B.: In order to consider cross couplings that originate from component tolerances in the LISNs and the attenuators, the

TABLE II
EXAMPLE VALUES FOR f_{DM} UND f_{CM}, CALCULATED WITH (33) AND (34), $DMTR = CMTR = 0$ DB, $DMRR = -68$ DB, AND $CMRR = -25$ DB. EXAMPLE NO. 1 IS BASED ON THE MEASUREMENT RESULTS DEPICTED IN FIGS. 12 AND 22(B), AT 270 kHz

No.	$V_{\mathrm{out,DM}}$	$V_{\mathrm{out,CM}}$	$V_{\mathrm{sep,DM,max}}$	$V_{\mathrm{sep,CM,max}}$	f_{DM}	f_{CM}
1	61 dBμV	66 dBμV	61.8 dBμV	66 dBμV	-14.8 dB	-67 dB
2	61 dBμV	76 dBμV	63.4 dBμV	76 dBμV	-6.4 dB	-77 dB
3	61 dBμV	86 dBμV	67.0 dBμV	86 dBμV	0 dB	-87 dB
4	131 dBμV	66 dBμV	131 dBμV	70.6 dBμV	-84 dB	-1.6 dB

frequency dependent functions $DMTR$, $CMTR$, $CMRR$, and $DMRR$ used to evaluate f_{DM} and f_{CM} depicted in Figs. 12(c), (d) and 16(c), (d) have been measured from the inputs of the LISNs to the outputs of the respective CM/DM separator, cf. Fig. 4, according to the measurement procedure outlined in the Appendix.

Table II lists examples for f_{DM} and f_{CM}, on the basis of the measurement results depicted in Fig. 12, evaluated at 270 kHz, for the LISNs connected in series to the attenuators and the separator of [2], cf. Fig. 22(b). Due to initial calibration $DMTR = CMTR = 0$ dB, $DMRR = -68$ dB, and $CMRR = -25$ dB apply. Example No. 1 uses the output voltages of Fig. 12 and examples No. 2 and 3 assume a successively decreasing attenuation of the CM filter, which leads to a successive increase of the CM output voltage from 66 to 86 dBμV. Example No. 1 represents a situation with relatively little cross coupling, i.e., useful estimations of $V_{\mathrm{sep,DM,max}}$ and $V_{\mathrm{sep,CM,max}}$ are feasible. In this situation f_{DM} und f_{CM} are less than -10 dB. With increasing magnitude of the CM output voltage the influence of $V_{\mathrm{out,CM}}$ on $V_{\mathrm{out,DM}}$ due to cross coupling gets increasingly pronounced. As a consequence, the reconstructed value $V_{\mathrm{sep,DM,max}}$ gets increasingly greater than the corresponding output voltage $V_{\mathrm{out,DM}}$, because the calculation of $V_{\mathrm{sep,DM,max}}$ assumes the worst case phasings of Fig. 11, and f_{DM} increases to a value of 0 dB in example No. 3. Example No. 3 represents a situation with maximum uncertainty regarding the value of the actually present DM input voltage, since the value measured for $V_{\mathrm{out,DM}}$ could result from cross coupling only, due to $CMRR\,V_{\mathrm{sep,CM}} = 61\,\mathrm{dB}\mu\,\mathrm{V} = V_{\mathrm{out,DM}}$, i.e., $V_{\mathrm{sep,DM}}$ could even be zero, cf. case I and (26). The opposite situation results for high values of $V_{\mathrm{out,DM}}$ and low values of $V_{\mathrm{out,CM}}$, cf., example No. 4 in Table II.

Based on these considerations and on the results listed in Table II the -6 dB limits

$$f_{\mathrm{DM}} < -6\,\mathrm{dB} \quad \text{and} \quad f_{\mathrm{CM}} < -6\,\mathrm{dB} \tag{35}$$

are considered to represent useful delimitations of meaningful measurement results for $V_{\mathrm{out,DM}}$ and $V_{\mathrm{out,CM}}$, respectively. For these limits and with the use of (33) and (34)

$$f_{\mathrm{DM}} < -6\,\mathrm{dB} \rightarrow\ V_{\mathrm{out,DM}} > 3\,V_{\mathrm{out,CM}}\,\frac{CMRR}{CMTR} \tag{36}$$

$$f_{\mathrm{CM}} < -6\,\mathrm{dB} \rightarrow\ V_{\mathrm{out,CM}} > 3\,V_{\mathrm{out,DM}}\,\frac{DMRR}{DMTR} \tag{37}$$

TABLE III
EQUIPMENT USED FOR THE MEASUREMENT OF CONDUCTED EMI. THE EXTERNAL ATTENUATORS FEATURE 10 DB ATTENUATION, SINCE THE LISN ALREADY PROVIDES 10 DB INTERNAL ATTENUATION

Measurement device	*Description*
LISNs	ENV216 by Rohde&Schwarz [25]
EMI test receiver	ESR3 by Rohde&Schwarz [26]
Attenuators	J01006A0836 by Telegärtner [27]

apply, i.e., the desired voltage component is at least three times greater than the unwanted voltage component that originates from cross coupling.

D. Evaluation with Measurement Data

Fig. 12(a) and (b) depicts measured DM and CM components, which have been obtained for the considered PFC rectifier, cf. Table I, with EMI filters in order to avoid excessive high-frequency load of the LISNs, using the measurement setup depicted in Fig. 4 and the equipment listed in Table III. The separator proposed by Paul and Hardin in [12] again provides output voltages that are approximately 5 dB below the output voltage measured with the separator proposed by Wang *et al.* in [2], which features an input impedance matrix close to $\underline{\mathbf{Z}}_{\mathrm{sep,ideal}}$. The measurement, however, also includes additional errors in the higher frequency range, e.g., due to limited ratios of $DMTR/CMRR$ and $CMTR/DMRR$. Still, the difference of approximately 5 dB is clearly apparent for DM and CM components.

Fig. 12(c) and (d) depicts the values of f_{DM} and f_{CM}, determined with (33) and (34), respectively. According to the conditions (36) and (37) cross coupling mainly influences the DM measurement result at high frequencies above approximately 15 MHz. However, DM noise components of less than 40 dBμV are obtained, there, i.e., considerably below the quasi-peak EMI limit of 60 dBμV (class B [3]), and for this reason the measurement error is in this case irrelevant for EMI filter design and verification.

IV. PERFORMANCE ACHIEVED WITH AN ACTIVE CM/DM SEPARATOR

A successful realization of a passive CM/DM separator includes careful optimization of broadband transformers and PCB layout in order to achieve acceptable separation capabilities in the required wide frequency range between 150 kHz and 30 MHz. The CM/DM separator, however, is subject to small signal excitations, i.e., the LISNs keep the supply currents away from it, and a passive CM/DM separator can be directly replaced by an active realization, which allows for a straightforward realization with relatively low effort, i.e., there is no need for cumbersome fine-tuning of the circuit.

A thorough literature review on active CM/DM separators reveals three publications showing general circuits of active CM/DM separators [17]–[19] and one master's thesis [16], which details the realization of an active CM/DM separator, however the CMRR of the presented circuit is reported to be

TABLE IV
COMPONENTS USED FOR THE ACTIVE CM/DM SEPARATOR

Designator	*Value*	*Description*
All resistors	Values given in Fig. 13	Chip resistors, 0805 case
Decoupling capacitors (not shown in Fig. 13)	100 nF	Chip capacitors, 0805 case, NP0
L_{CM}	1 mH	WE 744222 (Würth Elektronik)
$\mathrm{OP}_1 \ldots \mathrm{OP}_4$		AD8051 (Analog devices)

rather sensitive to trimmer adjustments. Fig. 13 depicts the proposed active CM/DM separator, which extends the original circuit by a CM-choke, L_{CM}, at the input of the differential amplifier formed with OP_4 in order to improve the circuit's properties with respect to CMRR. The considered circuit employs two operational amplifiers, OP_1 and OP_2, to realize an ideal input impedance matrix [together with $R_{\mathrm{in,l}}$ and $R_{\mathrm{in,n}}$, cf. (2)]. The resistive voltage divider formed with $R_{\mathrm{a},1}$ and $R_{\mathrm{a},2}$ provides the CM voltage, $(v_{\mathrm{sep},1} + v_{\mathrm{sep},2})/2$, to the input of OP_3 and OP_3 outputs this voltage to the test receiver. OP_4 provides the difference, $v_{\mathrm{sep},1} - v_{\mathrm{sep},2}$, at its output. The additional resistance $R_{\mathrm{d},5} = 50\,\Omega$ (realized with paralleling two $100\,\Omega$ resistors) causes the output voltage, $v_{\mathrm{out,DM}}$ to be divided by two, if the test receiver with its $50\,\Omega$ input impedance is connected, in order to obtain the DM-component according to (1). Fig. 14 depicts a picture of the realized device.

Adequate operational amplifiers and close-tolerance resistors need to be employed in order to achieve high-CM/DM separation capability. Furthermore, the operational amplifiers and the CM-choke are selected with regard to the frequency range of the application, $150\,\mathrm{kHz} \leq f \leq 30\,\mathrm{MHz}$. Table IV lists the used components. The employed low-cost operational amplifiers (AD8051) feature a unity gain bandwidth of 110 MHz and low distortion. At $f = 1\,\mathrm{MHz}$, their CM and power supply rejection ratios are -47 and -34 dB, respectively. The specified input voltage noise is $16\,\mathrm{n\,V}/\sqrt{\mathrm{Hz}}$ [28]. With this, a noise floor at approximately 33 dBμV results in Fig. 16, which is considerably less than the limits of conducted EMI ($56\,\mathrm{dB}\mu\mathrm{V} \ldots 66\,\mathrm{dB}\mu\mathrm{V}$).[6] The employed CM-choke is capable of a DM current of 800 mA and provides a CM impedance greater than $1\,\mathrm{k}\Omega$ in the considered frequency range, $150\,\mathrm{kHz} < f < 30\,\mathrm{MHz}$ [29]. All resistors and capacitors are SMD components in 0805 cases (100 nF/16 V/X7R ceramic capacitors—not shown in Fig. 13—are placed close to the supply pins of the operational amplifiers). The employed resistors have been initially measured and the most accurate components have been used. All $50\,\Omega$ resistors are realized with paralleling two $100\,\Omega$ resistors.

The active CM/DM separator is implemented on a standard two-layer PCB, with base material FR-4 and 35 μm thick copper planes on either side. The realized PCB layout of the active CM/DM separator respects the standard rules for best practice circuit design and, in particular, considers circuit's symmetries, e.g., equally long wires where applicable. Component placement and PCB layout are to a great extent shown in Fig. 14; the opposite copper layer of the PCB, which is not shown in Fig. 14, mainly forms a ground plane. A 9 V battery powers the shown circuit for more than $15\,h$, the measured supply current is 30 mA.

Due to zero inner impedance of the CM output port, a short cable between the CM output port and the EMI test receiver is recommended in order to avoid measurement errors due to reflections.

The separator's gain errors, $DMTR$ and $CMTR$, and cross-coupling characteristics, $CMRR$ and $DMRR$, have been measured with two power splitters (ZSCJ-2-2+ and ZSC-2-2+) according to the measurement method justified in the Appendix. Fig. 15 presents the values of $DMTR$, $CMTR$, $CMRR$, and $DMRR$ measured for the considered separator circuit and reveals that the active separator features competitive separation properties with $DMTR/CMRR > 50$ dB and $CMTR/DMRR > 42$ dB for frequencies up to 10 MHz. These results are similar to the separation capabilities found in [16], where $DMTR/CMRR$ between 30 and 55 dB (45 dB for $f < 1\,\mathrm{MHz}$ and 30 dB for $20\,\mathrm{MHz} < f < 30\,\mathrm{MHz}$) and $CMTR/DMRR$ between 53 and 90 dB (> 80 dB for $f < 1\,\mathrm{MHz}$ and close to 53 dB for $20\,\mathrm{MHz} < f < 30\,\mathrm{MHz}$) are reported. Different to the results of [16], the presented results have been achieved without initial fine tuning, which, with respect to $DMTR/CMRR$, is addressed to the use of the CM-choke, L_{CM}. Fig. 15 also depicts the corresponding phase responses of DMTR, CMTR, CMRR, and DMRR. Smooth phase responses result for DMTR and CMTR and the phase responses of CMRR and DMRR, in contrast, greatly change, which is addressed to the parasitic components and nonideal device properties that are responsible for the cross-coupling characteristics. It is to be noted that both, passive and active separators, typically provide adequate CM/DM discrimination capabilities in order to enable the diagnostic search for reasons for insufficient attenuations of an EMI filter. The passive separator is based on a simple circuit and does not require a power supply, however, careful initial calibration is typically required. By comparison, the proposed active separator features a better reproducibility of a defined performance, which comes at the cost of a more complex circuit. Thus, depending on the present measurement environment, either the passive or the active separator may be preferred.

Fig. 16 compares the DM and CM EMI spectra measured with the passive separator of [2] to the measurement result obtained with the proposed active separator. A visual inspection of these measurement results reveals only minor differences, e.g., the active separator generates a noise floor that is approximately 10 dB greater than that of the passive separator. Fig. 16(c) and (d) shows the corresponding results for f_{DM} and f_{CM}, calculated with (33) and (34). According to these results and the conditions (36) and (37), cross coupling does not considerably influence the measurement results of the active separator, may, however, have an impact on the DM components measured with the passive separator at frequencies greater than 15 MHz. Fig. 16(a) corresponds to this result, e.g., the peak visible for the passive separator at $f = 20\,\mathrm{MHz}$ does not appear for the active separator. However, in this case the spectral DM components that

[6] Fig. 16 depicts the measurement result plus 20 dB in order to compensate for the attenuators and to enable a comparison with known limits of conducted EMI. The noise floor of the realized active CM/DM separator itself is at 13 dBμV.

originate from cross coupling are less than the relatively high noise floor of the active separator.

V. Discussion

The below list briefly summarizes the findings of this paper.

1) In case of a nonideal or an unknown input impedance matrix of the employed CM/DM separator it is advisable to consider the measurement setup with precision attenuators depicted in Fig. 4 and to remove gain errors by means of an initial calibration (Section III-A). The attenuators may be omitted in case of a CM/DM separator with an ideal input impedance matrix; still, initial calibration is highly recommended.
2) LISNs realized with close-tolerance components need to be employed, since the output impedances of commercially available LISNs may be subject to rather high tolerances, which considerably deteriorates the measurement results (Section III-B1).
3) The value of the DM output signal is expected to be marginally affected by cross coupling at frequency f if $f_{\mathrm{DM}}(f) > 6$ dB applies, i.e., if $V_{\mathrm{out,DM}}(f)$ is greater than $3V_{\mathrm{out,CM}}(f)CMRR/CMTR$, cf. (33) and (36). The value of the CM output signal is expected to be marginally affected by cross coupling if $f_{\mathrm{CM}}(f) > 6$ dB applies, i.e., if $V_{\mathrm{out,CM}}(f)$ is greater than $3V_{\mathrm{out,DM}}(f)$ $DMRR/DMTR$, which is given with (34) and (37) and detailed in Section III-C.

It is noted that this work focuses on the magnitudes of the complex gain errors introduced by a nonideal input impedance matrix, $\underline{DMTR}$, $\underline{CMTR}$, $\underline{DMRR}$, and $\underline{DMRR}$, since IEC 61000-6-3 [3] only specifies limits for the amplitudes of conducted EMI and because the peak values of conducted EMI are expected to be independent of phase shift errors during processing, since same peak values result when the phasors of all spectral components in the measured 9 kHz frequency band of the EMI test receiver are in phase [23]. Phase information is usually not available from EMI test receivers and, for this reason, the indicators f_{DM} and f_{CM} are estimated for worst-case phase shift scenarios in Section III-C.

Fig. 17 depicts two flow-charts for guidance on how to apply the findings in this work. Fig. 17(a) shows the necessary steps to correct the gain error that arises from an unsuitable input impedance matrix of the employed CM/DM separator, cf. Section III-A. Fig. 17(b) presents a possible application of the indicators f_{DM} and f_{CM}, used to assess measurement errors due to cross coupling (DM and CM): In the course of the measurement of conducted EMI, using the setup of Fig. 4, f_{DM} and f_{CM} are calculated for the CM and DM voltage amplitudes measured at each frequency in order to determine, whether the separator's output values are largely influenced by cross coupling or not.

VI. Conclusion

Three contributions to the practical measurement of CM and DM components of conducted EMI are detailed. First, the implications of the impedance criterion given with (2) on the measurement errors are investigated. Analytical results obtained for a simplified model are verified by means of a more detailed model of the considered measurement setup and experimental results. According to the obtained results, only a gain error is expected in a practice oriented measurement configuration. The gain error can be removed by means of initial calibration.

This work further derives a method, which determines the worst-case measurement error by reason of cross coupling and for given measured DM and CM output voltage components. With the derived analytical expressions (33) and (34) it is straightforward to calculate how strong cross coupling affects the measurement result. A computer program may advantageously use the subsequently developed expressions (36) and (37) to automatically decide whether a particular spectral measurement component is strongly affected by cross coupling.

Finally, an active CM/DM separator is detailed, which features straightforward realization and competitive separation capability, $DMTR/CMRR > 50$ dB and $CMTR/DMRR > 42$ dB for frequencies up to 10 MHz. Experimental results reveal a good matching of the EMI spectra measured with passive and active separators.

Appendix

The separator's gain errors, $DMTR$ and $CMTR$, and cross-coupling characteristics, $CMRR$ and $DMRR$, have been measured according to [30]. This procedure requires two different power splitters, which split a given input signal into two output signals with same amplitude, with the output signals being either in phase or phase shifted by 180° (this work employs the two power splitters ZSC-2-2+ and ZSCJ-2-2+, manufactured by mini circuits). Since the power splitters introduce a measurement error themselves [2], their gains and cross-coupling characteristics are first measured in Appendix A in order to assure that the finally measured gains and cross-coupling characteristics of the separators are related to the separators and not to the power splitters. Appendix B presents the measurement results for $DMRR$, $CMRR$, $CMTR$, and $DMTR$ obtained for the active separator (inclusive LISN and attenuators), includes a comparison to the values obtained with an alternative measurement method presented in [2], and summarizes the measurement results for $DMRR$, $CMRR$, $CMTR$, and $DMTR$ obtained for the passive separators (inclusive LISN and attenuators). The separators' gain and coupling characteristics given in Figs. 20(a) and 22 have been used to determine the values of f_{DM} and f_{CM} that correspond to the respective separator, cf. Figs. 12(c), (d) and 16(c), (d).

A. Measured Output Characteristics of the Power Splitters

The output signals at both outputs of the investigated power splitter are measured in a subsequent manner, cf. Fig. 18(a) and (b). The phase correct addition or subtraction (and multiplication with $1/2$) of the measured output voltages $\underline{V}_{\mathrm{T1}}$ and $\underline{V}_{\mathrm{T2}}$ return the CM or DM components at the output of the splitters, respectively, which is related to the input voltage, $\underline{V}_{\mathrm{R}}$, in order to determine the CM and DM transfer functions of the

two power splitters (gain and phase) depicted in Fig. 19

$$\underline{G}_{\mathrm{CM}} = \frac{\underline{V}_{\mathrm{T1}} + \underline{V}_{\mathrm{T2}}}{2\underline{V}_{\mathrm{R}}} \text{ and } \underline{G}_{\mathrm{DM}} = \frac{\underline{V}_{\mathrm{T2}} - \underline{V}_{\mathrm{T1}}}{2\underline{V}_{\mathrm{R}}}. \quad (38)$$

The measurement results reveal that the power splitter ZSC-2-2+ (0°, specified frequency range: $2\,\mathrm{kHz} < f < 60\,\mathrm{MHz}$) achieves $G_{\mathrm{CM,ZSC-2-2+}}/G_{\mathrm{DM,ZSC-2-2+}} > 60$ dB in the relevant frequency range. The second power splitter, ZSCJ-2-2+ (180°, specified frequency range: $10\,\mathrm{kHz} < f < 20\,\mathrm{MHz}$), features $G_{\mathrm{DM,ZSCJ-2-2+}}/G_{\mathrm{CM,ZSCJ-2-2+}} > 60$ dB for $150\,\mathrm{kHz} < f < 2\,\mathrm{MHz}$ and $G_{\mathrm{DM,ZSCJ-2-2+}}/G_{\mathrm{CM,ZSCJ-2-2+}} > 38$ dB up to 30 MHz.[7] The phase responses of the separators' main output voltage components (CM for ZSC-2-2+ and DM for ZSCJ-2-2+) are $\arg(\underline{G}_{\mathrm{CM,ZSC-2-2+}})$ and $\arg(\underline{G}_{\mathrm{DM,ZSCJ-2-2+}})$ and are between 0 and -47°. Fig. 19 omits the phase corresponding to $\underline{G}_{\mathrm{DM,ZSC-2-2+}}$ for $f < 400\,\mathrm{kHz}$, due to the very small values of $G_{\mathrm{DM,ZSC-2-2+}}$, which leads to unusable phase information. The measured separation capabilities are considered to be sufficient regarding the employed CM/DM separators, in particular when DMTR, CMTR, CMRR, and DMRR consider the properties of the complete measurement chain (LISNs, attenuators, and separator).

B. DMTR, CMTR, CMRR, and DMRR Measured for LISNs, Attenuators, and Separators

Fig. 20 shows the gain errors and the cross-coupling characteristics from the inputs of the LISNs to the outputs of the active separator detailed in Section IV, i.e., from l and n to the separator's output ports in Fig. 4, measured with two different methods: Fig. 20(a) is obtained with the power splitters according to Fig. 18(c) and [30], where the measurement result is adjusted by the gain and phase transfer functions of the power splitters, cf. Fig. 19 and (38), in order to get the actual transmission and rejection ratios of the series connection of LISNs, attenuators, and separator; Fig. 20(b) is obtained by means of S-parameter measurements according to [2]. Both results reveal $DMTR = CMTR = -20$ dB, due to the employed 20 dB attenuators. Differences between the two measurements are clearly visible, e.g., the S-parameter method reveals greater values of $CMRR$ than the power splitter method for $f < 290\,\mathrm{kHz}$; furthermore, at the resonance visible at $f \approx 6.5\,\mathrm{MHz}$, the power splitters measure increased values of $DMRR$ and $CMRR$ and, with the S-parameter method, a decrease results in a narrow band around 6.5 MHz. However, both measurement methods are prone to measurement errors, in particular for great values of $DMTR/CMRR$ and $CMTR/DMRR$. This is due to the separation capabilities of the power splitters themselves and due to the accuracy of the measured S-parameters, since the expressions used to calculate $CMRR$ and $DMRR$, given in [2], are found to lead to differences of similar values if $DMTR/CMRR \gg 1$ and/or $CMTR/DMRR \gg 1$ apply. Due to this aspect and due to the power splitters being characterized in Fig. 19 the authors feel more confident with the results obtained with power splitters. Still, comparable characteristics and, with respect to a practical application, relatively high separation capabilities of more than 35 dB are measured for frequencies up to 10 MHz with both methods. Fig. 21, finally depicts the corresponding phase responses of DMTR, CMTR, CMRR, and DMRR. These phase responses are different to the phase responses depicted in Fig. 15, due to the different measurement setup, which, in Fig. 21, additionally includes LISNs and attenuators.

Fig. 22 presents the gain errors and separation characteristics and the corresponding phase responses of the passive separators used in this work. A discussion of the most important differences between the active and the two passive separators is listed below.

1) Fig. 20(a): The active separator features highest separation capabilities. At high frequencies ($f > 10\,\mathrm{MHz}$), however, resonance phenomena seem to occur, which is not the case for the two passive separators. Fig. 16 reveals that the active separator generates a higher noise floor than the passive separators.
2) Fig. 22(a): The passive separator presented in [12] achieves good separation capabilities of more than 40 dB up to approximately 3 MHz. At high frequencies the implemented separator is still usable, however, reduced separation capabilities, greater than 20 dB, are achieved.
3) Fig. 22(b): The employed implementation of the passive separator introduced in [2] achieves overall good separation of CM and DM components, except for a limited value of $DMTR/CMRR$ of less than 40 dB at frequencies less than 1 MHz, which, however, is addressed to the transducers used in this particular realization of the separator, since, according to [2], considerably better separation capability can be achieved with this circuit. The indicator $f_{\mathrm{DM}}(f)$, plotted in Fig. 12(d), reveals that the realized separator determines the spectral DM components with sufficient accuracy in this frequency range.
4) For DMTR and CMTR, similar phase responses result for all three measured separators.

[7] The amplitude responses depicted in Figs. 15, 20, and 22 use dashed lines for the measurement results obtained with the ZSCJ-2-2+ power splitter for frequencies greater than 20 MHz, due to operation above the specified frequency range.

REFERENCES

[1] S. Schroth, F. Krismer, J. W. Kolar, and H. Ertl, "Analysis and practical relevance of CM/DM EMI noise separator characteristics," *Proc. 16th Eur. Conf. Power Electron. Appl.*, Lappeenranta, Finland, Aug. 26–28, 2014, pp. 1–10.

[2] S. Wang, F. C. Lee, and W. G. Odendaal, "Characterization, evaluation, and design of noise separator for conducted EMI noise diagnosis," *IEEE Trans. Power Electron.*, vol. 20, no. 4, pp. 974–982, Jul. 2005.

[3] *Electromagnetic Compatibility (EMC) – Part 6: Generic Standards, Section 3: Emission Standard for Residential, Commercial and Light-industrial Environments, IEC 61000-6-3*, 2006.

[4] K. Raggl, T. Nussbaumer, and J. W. Kolar, "Model based optimization of EMC input filters," *Proc. IEEE 11th Workshop Control Model. Power Electron.*, Zürich, Switzerland, Aug. 18–20, 2008, pp. 1–6.

[5] *Specification for Radio Disturbance and Immunity Measuring Apparatus and Methods—Part 1: Radio Disturbance and Immunity Measuring Apparatus, Section 2: Ancillary Equipment – Conducted Disturbances, IEC/CISPR 16-1-2*, 2003.

[6] K. S. Kostov *et al.*, "The input impedance of common-mode and differential-mode noise separators," *IEEE Trans. Ind. Appl.*, vol. 51, no. 3, pp. 2352–2360, May/Jun. 2015.

[7] I. Kovacevic, F. Krismer, S. Schroth, and J. W. Kolar, "Practical characterization of EMI filters replacing CISPR 17 approximate worst case

measurements," *Proc. IEEE 14th Workshop Control Model. Power Electron.*, Salt Lake City, UT, Jun. 23–26, 2013, pp. 1–10.
[8] F. Luo, D. Dong, D. Boroyevich, P. Mattavelli, and S. Wang, "Improving high-frequency performance of an input CM filter using an impedance-mismatching filter," *IEEE Trans. Power Electron.*, vol. 29, no. 10, pp. 5111–5115, Oct. 2014.
[9] D. Boillat, F. Krismer, and J. W. Kolar, "Design space analysis and ρ–η Pareto optimization of LC output filters for switch-mode ac power sources," *IEEE Trans. Power Electron.*, vol. 30, no. 12, pp. 6906–6923, Dec. 2015.
[10] J. Qing, X. Ruan, and Z. Ye, "The worst conducted EMI spectrum of critical conduction mode boost PFC converter," *IEEE Trans. Power Electron.*, vol. 30, no. 3, pp. 1230–1241, Mar. 2015.
[11] M. J. Nave, "A novel differential mode rejection network for conducted emissions diagnostics," in *Proc. IEEE Natl. Symp. Electromagn. Compat.*, May 1989, pp. 223–227.
[12] C. R. Paul and K. B. Hardin, "Diagnosis and reduction of conducted noise emissions," *IEEE Trans. Electromagn. Compat.*, vol. 30, no. 4, pp. 553–560, Nov. 1988.
[13] K.Y. See, "Network for conducted EMI diagnosis," *Electron. Lett.*, vol. 35, no. 17, pp. 1446–1447, Aug. 1999.
[14] A. Nagel and R. W. De Doncker, "Separating common mode and differential mode noise in EMI measurements," *Proc. 8th Eur. Conf. Power Electron. Appl.*, Lausanne, Switzerland, Sept. 7–9, 1999, pp. 1–8.
[15] T. Guo, D.Y. Chen, and F.C. Lee, "Separation of the common-mode- and differential-mode-conducted EMI noise," *IEEE Trans. Power Electron.*, vol. 11, no. 3, pp. 480–488, May 1996.
[16] T. von Rauner, "A measurement system for evaluation of the coupling modes and mechanisms of conductive noise," M.S. thesis, Elect. Commun. Eng., Helsinki Univ. Technol., Helsinki, Finland, Jun. 1999.
[17] P.-S. Chen and Y.-S. Lai, "Software-based separation of conductive EMI signals," *Proc. IEEE Ind. Appl. Conf. 41st IAS Annu. Meeting*, Tampa, FL, USA, Oct. 8–12, 2006, vol. 3, pp. 1209–1214.
[18] M. L. Heldwein, J. Biela, H. Ertl, T. Nussbaumer, and J. W. Kolar, "Novel three-phase CM/DM conducted emissions separator," *IEEE Trans. Ind. Electron.*, vol. 56, no. 9, pp. 3696–3703, Sep. 2009.
[19] X. Chang, W. Chen, and X. Yang, "Performance improvement of CM/DM noise separator with impedance matching approach," *Proc. IEEE 29th Appl. Power Electron. Conf. Expo.*, Fort Worth, TX, USA, Mar. 16–20, 2014, pp. 3392–3396.
[20] J. Kelin, W. Jingmei, W. Chang, and B. Chuang, "A new method for conducted EMI noise diagnosis," *Proc. IEEE 8th Int. Conf. Electron. Meas. Instrum.*, Xi'an, China, Aug. 16–18, 2007, pp. 4-59–4-63.
[21] Y.-K. Lo, H.-J. Chiu, T.-H. Song, M.-P. Chen, and T.-S. Luor, "A software-based CM and DM measurement system for the conducted EMI," *Proc. 25th Annu. Conf. IEEE Ind. Electron. Soc.*, San Jose, CA, USA, Nov. 29–Dec. 3, 1999, vol. 1, pp. 253–255.
[22] J. Stahl, D. Kuebrich, and T. Duerbaum, "Modification and characterization of a standard LISN for effective EMI noise separation," *Proc. IEEE Int. Conf. Electromagn. Adv. Appl.*, Sydney, NSW, Australia, Sept. 20–24, 2010, pp. 39–42.
[23] M. L. Heldwein, "EMC filtering of three-phase PWM converters," Ph.D. dissertation, no. 17554, ETH Zürich, 2008.
[24] K. Raggl, T. Nussbaumer, and J. W. Kolar, "Guideline for a simplified differential-mode EMI filter design," *IEEE Trans. Ind. Electron.*, vol. 57, no. 3, pp. 1031–1040, Mar. 2010.
[25] Rohde&Schwarz GmbH & Co. KG. R&S ENV216 Two Line V-Network Betriebshandbuch. Accessed on: April, 2016. [Online]. Available: https://cdn.rohde-schwarz.com/pws/dl_downloads/dl_common_library/dl_manuals/gb_1/e/env216_1/5201669314_0300_MAN_1_DE_EN.pdf
[26] Rohde&Schwarz GmbH & Co. KG. R&S ESR EMI Test Receiver Specifications. Accessed on: April, 2016. [Online]. Available: https://cdn.rohde-schwarz.com/pws/dl_downloads/dl_common_library/dl_brochures_and_datasheets/pdf_1/service_support_30/ESR_dat-sw_en_3606-7201-22_v0400.pdf
[27] Telegärtner Karl Gärtner GmbH. Data sheet information on the 10 dB BNC attenuator J01006A0836. Accessed on: April, 2016. [Online]. Available: http://mediando.telegaertner.com/?IdTreeGroup=12995&IdProduct=533&lang=de&pdf=true
[28] Analog Devices Inc. Data sheet information on the AD8051/AD8052/AD8054 operational amplifiers. Accessed: March, 2016. [Online]. Available: http://www.analog.com/media/en/technical-documentation/data-sheets/AD8051_8052_8054.pdf
[29] Würth Elektronik GmbH & Co. KG. Data sheet information on the WE-SL2 SMD Common Mode Line Filter, no. 744222. Accessed: March, 2016. [Online]. Available: http://katalog.we-online.de/pbs/datasheet/744222.pdf
[30] M. C. Caponet, F. Profumo, L. Ferraris, A. Bertoz, and D. Marzella, "Common and differential mode noise separation: comparison of two different approaches," *Proc. IEEE 32nd PESC 2001*, Vancouver, BC, Canada, pp. 1383–1388, 17–21 Jun. 2001.
[31] Keysight Technologies Inc. Data sheet information on the Keysight E5061B Network Analyzer. Accessed on: April, 2016. [Online]. Available: http://literature.cdn.keysight.com/litweb/pdf/5990-4392EN.pdf?id=1790097

Florian Krismer (M'12) received the Dipl.-Ing (M.Sc.) degree in electrical engineering with specialization in automation and control technology from the Vienna University of Technology, Vienna, Austria, in 2004, and the Ph.D. degree in electrical engineering from the Department of Information Technology and Electrical Engineering of ETH Zürich, Zurich, Switzerland, in 2010.

He is currently a Research Associate at PES, where he has co-supervised Ph.D. students and has continued with his research in the field of power electronics. He is the author or coauthor of numerous conference and peer-review publications and has received two awards for his publications. His research interests include the analysis, design, and general optimization of power converter systems, e.g., the weight optimization of a bi-directional dc–dc converter for an airborne wind turbine. Furthermore, he conducts research related to the filtering of conducted electromagnetic emissions and collaborated in the littlebox-challenge with respect to the hardware realization.

Sebastian Schroth received the Diploma degree in electrical engineering and information technology from the University of Stuttgart, Stuttgart, Germany, in 2011.

From 2011 to 2014, he had been a Research Assistant at the Power Electronic Systems Laboratory, Swiss Federal Institute of Technology, Zurich, Switzerland, with a focus on EMC in electrical drives. Since November 2014, he has been with ebm-papst Mulfingen GmbH & Co. KG, Germany, where he continues his research in EMC of electrical drives and fans.

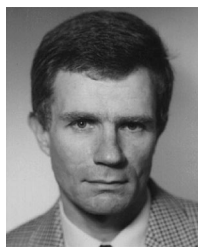

Hans Ertl (M'93) received the Dipl.-Ing. (M.Sc.) and the Ph.D. degrees in industrial electronics from the University of Technology Vienna, Vienna, Austria, in 1984 and 1991, respectively.

Since 1984, he has been with the Vienna University of Technology, Vienna, Austria, where he is currently an Associate Professor with the Power Electronics Section of the Institute of Electrical Drives and Machines. He has performed numerous industrial and scientific research projects in the areas of field-oriented control of ac drive systems, switch-mode power supplies for welding and industrial plasma processes, and active rectifier systems. He is the author or coauthor of numerous scientific papers and patents. His current research interests include switch-mode power amplifiers and multicell topologies, in particular, for the generation of testing signals, for active ripple current compensators, and for several applications in the area of renewable energy systems.

Konstantin Stoychev Kostov (SM'16) received the M.Sc., Lic.Sc., and D.Sc. (Tech.) degrees in electrical engineering from the Helsinki University of Technology, Helsinki, Finland, in 2003, 2006, and 2009, respectively.

In 2011, he moved to Stockholm, Sweden, for a two year Post-Doc position at the Department of Electrical Energy Conversion, KTH Royal Institute of Technology. Since September 2013, he has been a Senior Scientist at Acreo Swedish ICT, in Kista, Sweden. His research interests include design, modeling, and control of power electronic converters, EMC in power electronics, and the packaging of high-power semiconductor devices.

Hans-Peter Nee (S'91–M'96–SM'04) was born in Västerås, Sweden, in 1963. He received the M.Sc., Licenciate, and Ph.D. degrees in electrical engineering from the KTH Royal Institute of Technology, Stockholm, Sweden, in 1987, 1992, and 1996, respectively.

Since 1999, he has been a Professor of power electronics with the Department of Electrical Engineering, KTH Royal Institute of Technology. His research interests include power electronic converters, semiconductor components, and control aspects of utility applications, such as FACTS and high-voltage direct-current transmission, and variable-speed drives.

Dr. Nee was a Member of the Board of the IEEE Sweden Section for many years and was the Chair of the Board from 2002 to 2003. He is also a Member of the European Power Electronics and Drives Association and is involved with its Executive Council and International Steering Committee.

Johann Walter Kolar (F'10) received the M.Sc. and Ph.D. degrees (*summa cum laude*/promotio sub auspiciis praesidentis rei publicae) from the Vienna University of Technology, Vienna, Austria, in 1997 and 1999, respectively.

Since 1984, he has been working as an Independent Researcher and International Consultant in close collaboration with the University of Technology Vienna, in the fields of power electronics, industrial electronics, and high-performance drives. He has proposed numerous novel PWM converter topologies, and modulation and control concepts, and has supervised more than 60 Ph.D. students. He has published more than 650 scientific papers in international journals and conference proceedings, 3 book chapters, and has filed more than 120 patents. The focus of his current research is on ultra-compact and ultra-efficient SiC and GaN converter systems, wireless power transfer, solid-state transformers, power supplies on chip, and ultra-high speed and bearingless motors.

Dr. Kolar received 21 IEEE Transactions and Conference Prize Paper Awards, the 2014 IEEE Middlebrook Award, and the ETH Zurich Golden Owl Award for excellence in teaching. He initiated and/or is the founder of four ETH Spin-off companies. He is a Member of the Steering Committees of several leading international conferences in the field and has served from 2001 through 2013 as an Associate Editor of the IEEE TRANSACTIONS ON POWER ELECTRONICS. Since 2002, he has also been an Associate Editor of the *Journal of Power Electronics* of the Korean Institute of Power Electronics and a Member of the Editorial Advisory Board of the IEEJ Transactions on Electrical and Electronic Engineering.